Spring 5-12-2018

Analysis of Double-Wall and Twisted-Tube Heat Exchanger Concepts for use in Fluoride Salt-Cooled High-Temperature Reactors

Bryan M. Wallace
University of New Mexico

Bryan Wallace

Candidate

Nuclear Engineering

Department

This thesis is approved, and it is acceptable in quality and form for publication:

Approved by the Thesis Committee:

Dr. Edward Blandford , Chairperson

Dr. Amir Ali

Dr. Youho Lee

Analysis of Double-Wall and Twisted-Tube Heat Exchanger Concepts for use in Fluoride Salt-Cooled High-Temperature Reactors

by

Bryan Wallace

B.S., Physics
Central Michigan University, 2015

THESIS

Submitted in Partial Fulfillment of the
Requirements for the Degree of

Master of Science
Nuclear Engineering

The University of New Mexico

Albuquerque, New Mexico

May, 2018

Dedication

To my parents, Donald and Therese, for their unconditional love and their unwavering support.

Acknowledgments

I'd like to acknowledge the great help and support that all of my colleagues and friends have constantly offered throughout my time in New Mexico. I'd first like to thank my advisor Dr. Ed Blandford for offering me the opportunity to learn from and work with him.

I would next like to thank my colleagues Dr. Joel Hughes for his mentorship and direction in heat transfer, Floren Rubio for his thoughts, ideas, problem solving skills and quote "Research is way more interesting when it isn't yours.", Dr. Maolong Liu for his expertise in heat transfer systems and instrumentation, and Dr. Amir Ali for pushing me throughout my time at UNM and for helping me through the many crises in the final stages of my degree. An extra mention is deserved for Joel, Floren, and Maolong for being great biking company.

I also want to thank my good friends and roommates Edward Hietter, John Tener, and our many foster dogs. Their constant friendship was a huge relief from the many stresses associated with earning a graduate degree.

Finally, I want to thank all of my other friends including those from Michigan and those that I made while here in New Mexico.

Analysis of Double-Wall and Twisted-Tube Heat Exchanger Concepts for use in Fluoride Salt-Cooled High-Temperature Reactors

by

Bryan Wallace

B.S., Physics
Central Michigan University, 2015

M.S., Engineering, University of New Mexico, 2017

Abstract

Fluoride Salt-cooled High-temperature Reactors (FHRs) are an attractive fourth generation reactor concept. Like other fourth generation concept designs, FHRs offer characteristics such as a high-temperature low-pressure molten salt coolant allowing the reactor to be combined with a high-temperature high-efficiency power generation cycle such as an air-Brayton or supercritical carbon dioxide (SCO_2).

Like most Gen IV reactor concepts, there are a few problems which need to be addressed with the design before it can be licensed. One particular design is the Mark 1 pebble bed FHR, a design put out by the University of California Berkeley. Two problems that need to be addressed are due to characteristics of the choice of molten salt. The main choice is a mixture of lithium fluoride and beryllium fluoride (flibe). This work attempts to analyze the heat transfer performance of a double wall twisted tube heat exchanger which could play a part in the solution to these problems.

Particularly, the focus of the work attempts to understand the performance of a three fluid, parallel stream heat exchanger with two thermal communications with an emphasis on understanding the effect the intermediate fluid and it's flow rate has on the overall effectiveness of the heat exchanger.

Contents

List of Figures

List of Figures

List of Tables

Chapter 1

Introduction

This chapter serves as an introduction to Fluoride Salt-Cooled High-Temperature Reactor (FHR) systems and delves into some of the technical challenges which may be holding the concept back from commercialization. The challenges focused on here are a result of a particular reactor design's chosen coolant type and its impact on heat transfer and production of tritium. The motivation and scope round this chapter off.

1.1 Fluoride Salt-Cooled High-Temperature Reactors

The FHR is a class of generation IV reactor concepts which the Department of Energy is interested in funding research towards. The FHR combines many technological advancements which the Molten Salt Reactor Experiment (MSRE), the first molten salt reactor, did not have. These advancements bring the concept to the forefront of reactor technology. Figure 1.1 depicts the key characteristics of the FHR including the aforementioned advancements.

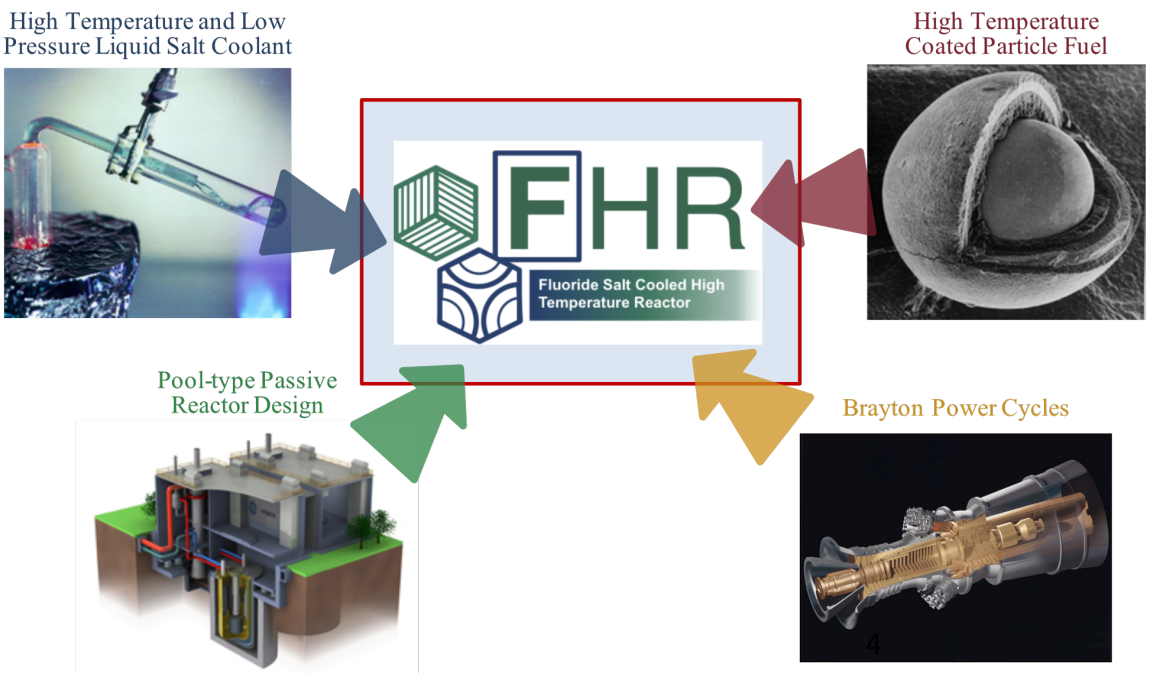

Figure 1.1: The four defining characteristics of the FHR.

There are multiple system designs which exist, however the FHR generally features a high temperature low pressure fluoride salt as a coolant, an advanced power generation cycle such as the open-air Brayton or supercritical CO_2 cycle, a tristructural isotropic (TRISO) fuel particle, and a pool-type passive decay heat removal system. The combination of these systems is seen as a large boost to system safety, reliability, and efficiency.

The Mark-1 Pebble Bed Fluoride Salt-Cooled High-Temperature Reactor (PB-FHR) [3] is the design which all calculations and motivations in this work have been based on. Notably, this design utilizes a constant circulation of floating TRISO particles to fuel the reactor. The system is highly beneficial with the capability to constantly fuel the reactor without requiring shutdown. It also allows for the online removal of damaged or depleted particles and addition of new fuel pebbles when needed.

Table 1.1: Candidate salts for the FHR, based on several tables in [2]. Thermophysical properties were evaluated at 700 $^{\circ}C$ except for vapor pressure, which was evaluated at 900 $^{\circ}C$.

Salt	T_{melt} $^{\circ}C$	T_{boil} $^{\circ}C$	P_{vapor} Pa	ρ $\frac{kg}{m^3}$	C_p $\frac{J}{kg-K}$	$\rho \times C_p$ $\frac{MJ}{m^3-K}$	μ $Pa-s$	λ $\frac{W}{m-K}$
LiF-BeF_2	458	~ 1400	160	1940	2420	4.69	0.0056	1.0
LiF-NaF-KF	454	1570	~ 90	2020	1880	3.81	0.0029	0.92
NaF-BeF_2	340	~ 1400	190	2010	2180	4.38	0.007	0.87
NaF-ZrF_4	500	~ 1350	670	3140	1170	3.68	0.0051	0.49
RbF-ZrF_4	410	~ 1450	170	3220	837	2.70	0.0051	0.37

The Mark-1 has chosen a eutectic mixture of ^7LiF and BeF_2 (flibe) as its baseline salt coolant. Molten salts are particularly attractive as a reactor coolant for their chemical stability, high melting and boiling temperatures, large thermal heat capacity, and lack of parasitic neutron capture. Table 1.1 provides the thermal properties of candidate molten salts for the FHR.

Figure 1.2 depicts the basic thermal hydraulic layout of the Mark-1. The Mark-1 utilizes two systems for removing heat from the core. The main salt piping system nominally uses two loops to directly heat air for the natural gas air combined cycle (NACC). During normal operation, the core outlet temperature of flibe reaches $700^{\circ}C$. The main salt piping system uses two coiled tube air heaters (CTAHs) nominally rated for half of the reactor's power production at 116 MWt each to heat air to $670^{\circ}C$.

The second system is the direct reactor auxiliary cooling system (DRACS). The three DRACS loops are intended to remove decay heat under emergency conditions when normal shutdown is not functional. Each loop is intended to remove 1 percent of the nominal power of the reactor (236 MW). The DRACS loops are also filled with flibe to prevent contamination of the primary salt in the event of a leak. Constantly operating under natural circulation conditions, the DRACS loop utilizes a salt-salt heat exchanger (DRACS heat exchanger, DHX) within the primary containment and a natural draft heat exchanger (NDX) to cool the DRACS salt loop.

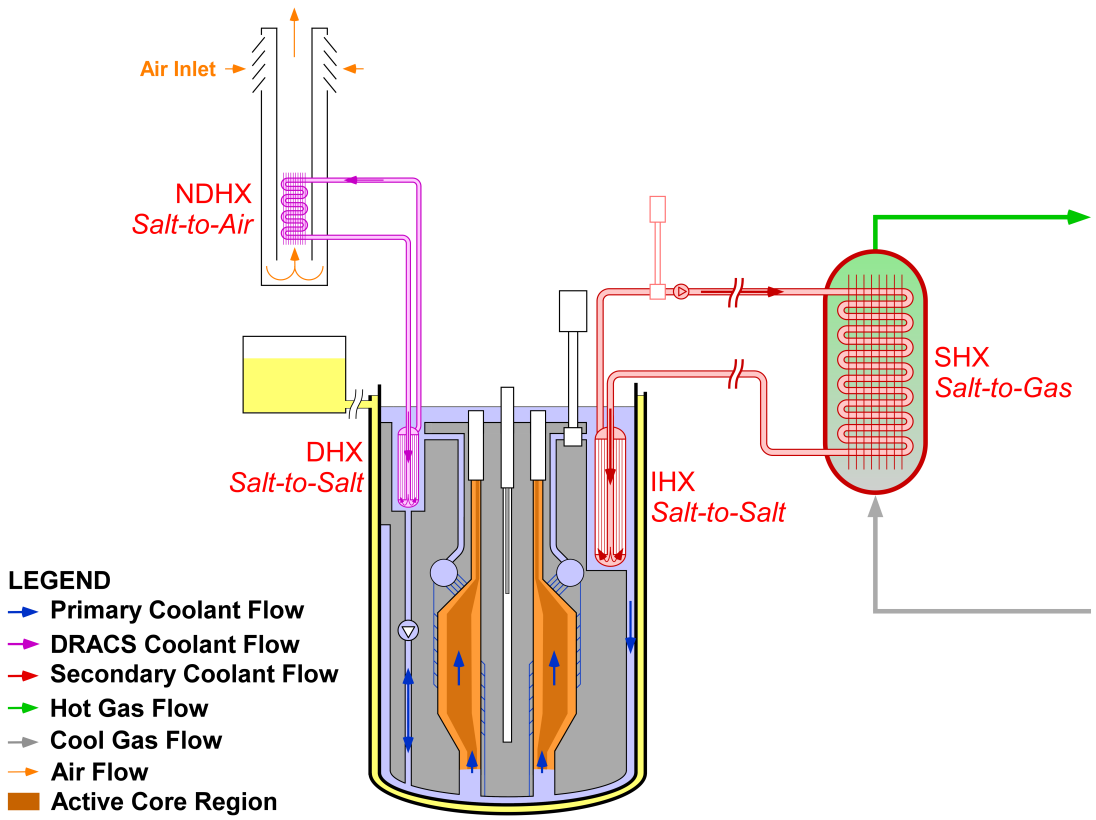

Figure 1.2: Notional diagram of the FHR

1.2 Motivation and Scope

In briefly discussing the design concept of the Mark-1 PB-FHR, a few of the technical challenges associated with this design can now be addressed, as resolving these issues are the motivation for this work.

1.2.1 High Prandtl Fluids

The challenges addressed here are a result of the Mark-1's choice of baseline coolant, flibe. Compared to water, flibe and other molten salts have appreciably higher heat capacity, melting, and boiling points. Molten salts also tend to have larger Prandtl numbers (Pr). Large heat capacities provide the benefit of fluids handling thermal transients better and high melting and boiling points allow for the reactor to use more efficient power generation cycles such as air Brayton or SCO_2. However, high Pr numbers can impose a penalty to heat transfer. The Pr number is a characterization of the relationship between the momentum and thermal boundary layers. As the Pr number increases, the width of the thermal boundary layer decreases. At first thought, this appears to be beneficial as one would think a small boundary layer would lead to better heat transfer. As the width of the thermal boundary layer decreases, the gradient of the boundary becomes more extreme within the momentum boundary layer. The thermal boundary layer is pushed towards the wall and into the laminar layer of the momentum boundary. The mixing of the boundary layers with the bulk fluid is poor here which can result in degraded heat transfer. Figure 1.3 depicts the effects of the Pr number on these boundary layers.

It is, therefore, advantageous to pursue heat transfer performance enhancement via advanced heat exchanger designs. Twisted-tube heat exchangers have been used in a variety of applications with large Pr fluids including food processing and the petrochemical industry. Twisted-tubes differ from their plain-tube counterparts in their ability to induce swirl as the shell-side and tube-side fluids pass through the heat exchanger, breaking up momentum and thermal boundary layers. This induced swirl can produce turbulent flow at lower Reynolds (Re) numbers and results in enhanced heat transfer performance. Twisted-tube heat exchangers may then be used in multiple heat exchanger positions throughout the thermal hydraulic system of the FHR but are of initial interest to be used in the DHX.

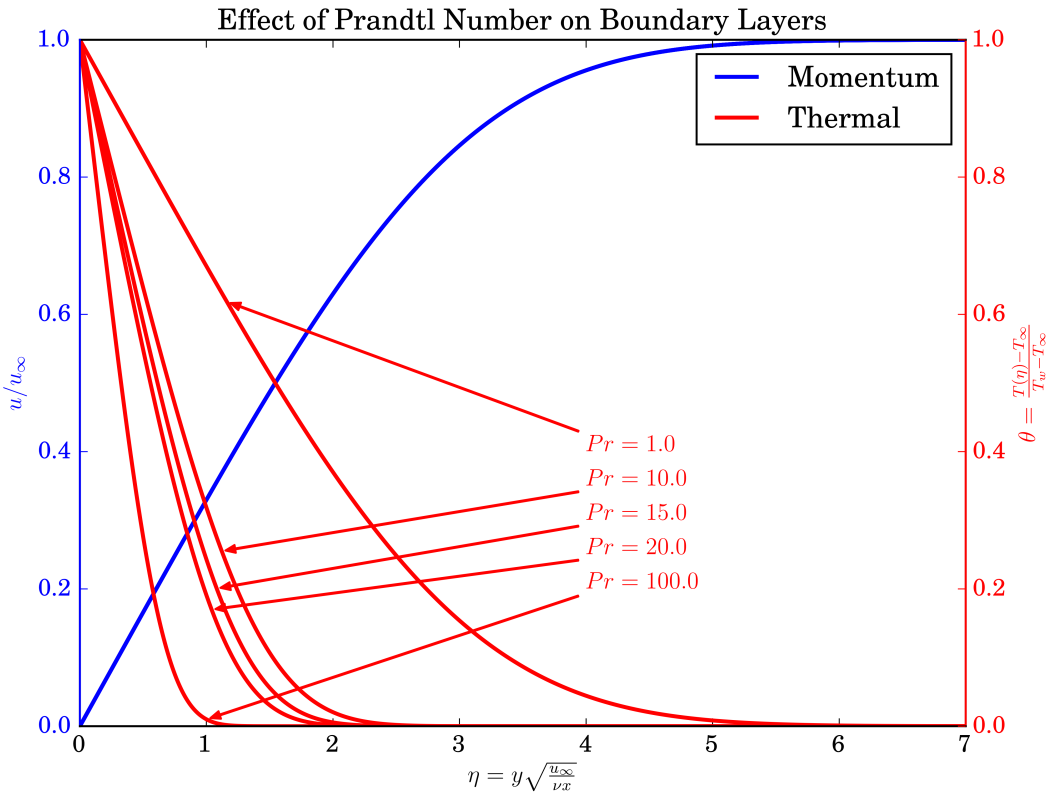

Figure 1.3: Effect of the Prandtl number on the thermal boundary layer as compared to the momentum boundary layer. The plot is for flow over a flat plate at zero instance. The plate is heated and the effect due to friction heating is ignored. This plot was based on information provided in [1].

1.2.2 Tritium Production and Release Mitigation

Equations 1-5 describe neutron interactions with flibe. Flibe is enriched to 99.995 % ^7Li, however residual amounts of ^6Li and production of ^6Li from eqs. 1d and 1e results in significant amounts of tritium being born. According to Stempien [4], initial estimates of tritium production in the Mark-1 could be as high as 3000 Ci t/GWt/d with the reactor at steady state. As mentioned, the FHR operates at 700°C. At this temperature, hydrogen and its isotopes permeate readily through stainless steels and

metals used in the thermal hydraulic system. Tritium is produced in the core and may be in the form of T_2, HT, or TF and may undergo multiple interactions with the coolant or the TRISO fuel pebbles before being transported throughout the reactor by the primary and intermediate coolant loops and the power conversion cycle. Heat exchangers, with their large surface area, are a prominent path which tritium may use to migrate from one loop to the next. A double-wall heat exchanger (DWHE), with its added walls and annular volume, may function as a part of the solution to preventing this migration. DWHEs have been traditionally used in applications where the prevention of two fluids mixing is mandatory. For example, DWHEs have been used in sodium fast reactor (SFR) steam generators. The added wall is another barrier to the prevention of molten sodium mixing with water and steam. As proposed by Gilman [5], tritium mitigation options for DWHEs include the use of permeation barriers, sweep gases, tritium getters, and fluids with an affinity for tritium such as liquid lithium.

Heat and mass transfer are directly related. Conditions which are ideal for the transfer of heat such as heat exchangers with large surface areas and convective heat transfer, are likely to be ideal for mass transfer. There are multiple ways to attempt to prevent tritium permeation through heat exchanger walls however, each will add thermal resistance and hinder the heat transfer between working fluids. It is necessary then to be able to assess each mitigation option in terms of their effectiveness at reducing tritium permeation, penalty they provide to heat transfer, cost, and other factors specific to each option such as compatibility with flibe of the permeation barriers.

$$^{6}LiF + n \rightarrow {}^{4}_{2}He + {}^{3}_{1}HF \tag{1.1a}$$

$$^{7}LiF + n \rightarrow {}^{4}_{2}He + {}^{3}_{1}HF + n' \tag{1.1b}$$

$$^{19}_{9}F + n \rightarrow ^{17}_{8}O + ^{3}_{1}H \tag{1.1c}$$

$$^{9}_{4}BeF_2 + n \rightarrow ^{4}_{2}He + ^{6}_{2}He + 2F \tag{1.1d}$$

$$^{6}_{2}He \rightarrow ^{6}_{3}Li + e^{+} + \bar{v}_e \tag{1.1e}$$

Permeation Barriers

From a heat transfer standpoint, permeation barriers add the least amount of thermal resistance of all mitigation methods. They can be applied to heat exchanger tubes as thin ceramic or metallic coatings. There are multiple materials which show promise as permeation barriers including Al_2O_3, SiO_2/SiC and TiN. Permeation barriers are rated based on their permeation reduction factor (PRF). This factor characterizes the percent reduction in the amount of tritium which permeates through a base material before and after barrier application. These materials have been shown to reduce hydrogen (and hydrogen isotopes) permeation by factors from 10 to 10000 [6]. The effectiveness of barriers is dependent on the thickness of the barrier, the presence of defects, and thermal compatibility to the base material (expansion differences and thermal shock response). Forcey [7] found Al_2O_3 coatings on 316L discs could provide PRFs up to 10000. Oxides are also attractive for their "self healing" properties. Should the oxide barrier be damaged, it is possible for the material to reoxidize.

Though permeation barriers are attractive, it does not appear that they can function as the sole solution to the prevention of tritium permeation. Many of these barriers are not compatible with molten salts and therefore would need to be applied to the tube-side of the heat exchanger. Also, Stempien studied the effects of applied barriers on heat exchanger surfaces using his developed code, TRIDENT, for

estimating tritium production and effectiveness of proposed solutions. He found that permeation barriers did not reduce the amount of tritium released from the reactor at steady state. The barriers simply raised the threshold for the amount of tritium held within the core before ultimately permeating through the heat exchanger. In order to prevent tritium from permeating, another system must be deployed to remove tritium from the core.

Sweep Fluids

Sweep gases and all other mitigation methods surrounding the heat exchanger except for permeation barriers call for the use of DWHEs. These options require an annular space between the primary (molten salt) and secondary (power generation) working fluids. Sweep gases could be implemented within this annular region. As the gas flows through the heat exchanger, tritium is picked up upon entry and is swept out before reaching the secondary side. As tritium is picked up, heat is also transferred to the inert gas and not to the secondary fluid decreasing the efficiency of the heat exchanger and the reactor plant. It therefore makes sense to choose the inert gas with the highest thermal conductivity, which is helium.

The inert gas can be modified with other gases to form chemical bonds with the tritium. These options such as hydrogen or oxygen could be used to more efficiently capture and hold on to tritium. This method however makes ultimate removal and storage of tritium more difficult. Working with these gases poses added risks and challenges. Hydrogen is, of course, extremely flammable and has its own potential for permeation into the reactor or out to the atmosphere through the power generation cycle. The piping system material has not been chosen yet however, using oxygen has the potential to oxidate these surfaces and further hinder the heat transfer process.

Another suggested option for a fluid in the annular gap is liquid lithium. Lithium

has a high affinity for tritium and has better heat transfer properties than any proposed sweep gas. Lithium therefore would be the best option from a heat transfer and power generation standpoint. Like other alkali metals, lithium is highly reactive and flammable. Therefore, it creates significant problems for handling and added risks in the event of a pipe break or other loss of coolant accident (LOCA).

Tritium Getters

Tritium getters provide a means for direct capture of tritium within the heat exchanger. Some metals, when exposed to hydrogen (and its isotopes) bond with the hydrogen at low partial pressures to create a metal hydride (tritide). These metals such as zirconium, titanium, and yttrium could fill the annular region as a metal powder or pebble form for the capture of tritium [6]. This method however, may force the heat exchanger to have a finite lifetime as the metal has a finite capacity for the capture of tritium. Once it approaches this capacity, it may fail to capture tritium as effectively, allowing it to permeate into the secondary fluid. There are ways to mitigate this problem. A possible solution would be to anneal the hydride within the annular space during reactor shutdown to release the tritium and allow it to be moved to another location. This could allow the heat exchanger to be used for multiple cycles before being replaced, if need be.

Other Mitigation Options

The FHR community is considering many other options for the capture or removal of tritium from the coolant and power generation cycle. One of those options is carbon capture. There are already sources of carbon within the proposed FHR facility including in the TRISO particle fuel pebbles. A proposed system of carbon capture involves flowing the molten salt through a packed bed of carbon pebbles before the

salt reaches the IHX. This solution is attractive as it shows promise as being able to remove large amounts of tritium from the salt. It has the same problems as the tritium getter within the heat exchanger. At some point the carbon pebbles may become saturated with tritium and will no longer remove tritium from the salt before it reaches the heat exchanger. This problem could be solved in multiple ways though. The packed bed could simply be large enough that the pebbles will not saturate with tritium in the reactors lifetime. As this section is separate from the heat exchanger, it is not confined by space. This however, will significantly increase costs from the large amount of space and materials including the increase in salt volume required to run the reactor. The pebbles could also float through the molten salt similar to the system for fueling the FHR. An online system of adding new pebbles and removing saturated pebbles from the salt. This system adds a significant layer of complexity to the plant.

Another possible mitigation option uses inert gas sparging to remove tritium from the coolant. In systems where a gas is dissolved within a liquid, a different inert gas can be bubbled through the liquid to remove the dissolved gas. The dissolved gas diffuses into the inert gas bubble and can then be easily separated from the liquid. The product is a mixture of inert gas and tritium which can be transported to another system for ultimate capture and disposal. Initial estimates by Stempien [4] show that this system would require extreme amounts of inert gas, in his testing helium, on the order of 20,000 L/hr.

1.2.3 Scope

The work described here attempts to analyze and evaluate the heat transfer performance for multiple heat exchangers. The aim of the first experiment performed is to calculate the nondimensional Nusselt number, a measure of heat transfer performance, of a plain tube shell-and-tube heat exchanger. Results for this experiment

are combined with that of Joel Hughes'[8] twisted tube tests to characterize the enhancement in heat transfer performance that twisted tubes provide. The second experiment performed is to characterize the impact which the addition of a second wall adds in heat transfer performance. In relation to tritium permeation mitigation, the sweep gas method allows for the capture of tritium outside of the reactor which is advantageous. This experiment attempts to simulate this solution and characterize the impact it has on heat transfer performance. This double-wall heat exchanger [1] has been modeled via a 1D code based on the conservation of energy and results have been obtained and compared to the experimental results for validation of the model.

[1]Double-wall heat exchangers, in their simplest form, are known as three-fluid heat exchangers in this work

Chapter 2

Mathematical Modeling of Thermal Hydraulic Phenomena

This chapter will provide some basic background in heat transfer as well as the modeling of thermal hydraulic phenomena including heat transfer and pressure drop in plain, twisted, and double-wall heat exchangers. Two-fluid heat exchangers are the most common and there is plenty of literature describing how to model these heat exchangers via the log mean temperature difference and effectiveness methods. Three-fluid heat exchangers (3FHE) are significantly less common, heat transfer and metrics for determining effectiveness will be discussed here.

2.1 Heat Exchanger Theory

Heat exchangers are used in a large variety of processes and as such, are very well characterized. Heat transfer and pressure drop are important metrics in determining the performance of a heat exchanger.

2.1.1 Pressure Drop

As the heat transfer fluid flows through a heat exchanger, friction and effects from the heat exchanger geometry can inflict pressure drop on the fluid. This may result in increased heat transfer in some cases but at a cost for increased pumping power. Correlations for predicting the pressure drop for plain and twisted tubes are found here.

Plain Cylindrical Tube

The Darcy-Weisbach correlation [9] predicts the pressure drop for plain tubes ΔP, per unit length L, of flowing fluid in a straight circular tube of uniform diameter D, with an average velocity V, due to viscous effect is given by:

$$\frac{\Delta P}{L} = \frac{f_D}{D}\frac{V^2}{2g} \tag{2.1}$$

The Churchill equation [10] for the Darcy friction factor f_D, can be used for the full range of Reynolds numbers (Re) (laminar, transition and turbulent) and roughness to diameter ratio, e/D:

$$f_D = 8\left[\left(\frac{8}{Re}\right)^{12} + \frac{1}{(A+B)^{1.5}}\right]^{\frac{1}{12}} \tag{2.2}$$

Where

$$A = \left[-2.457\ \ln\left(\left(\frac{7}{Re}\right)^{0.9} + 0.27\left(\frac{e}{D}\right)\right)\right]^{16} \tag{2.3}$$

and

$$B = \left(\frac{37530}{Re}\right)^{16} \tag{2.4}$$

In the laminar regime (Re < 2000), f_D is independent of the surface roughness and is given by the Stokes formula [9]

$$f_D = \frac{64}{Re} \tag{2.5}$$

Twisted Tube

There is much less information on twisted tubes in the literature. There are a significant amount of parameters which are important in the correlations for pressure drop and heat transfer and as such, they can be found below [8]:

$$F_\Sigma = \pi \frac{d_{shell}^2}{4} \tag{2.6}$$

$$F_s = F_\Sigma - \frac{N\pi \; d_{max,out} \; d_{min,out}}{4} \tag{2.7}$$

$$\Pi'_{in} = \pi \left(3(r_{max,in} + r_{min,in}) - \sqrt{(3r_{max,in} + r_{min,in})(r_{max,in} + 3r_{min,in})}\right) \tag{2.8}$$

$$\Pi'_{out} = \pi \left(3(r_{max,out} + r_{min,out}) - \sqrt{(3r_{max,out} + r_{min,out})(r_{max,out} + 3r_{min,out})}\right) \tag{2.9}$$

$$r_{out,e} = \frac{\Pi'_{out}}{2\pi} \tag{2.10}$$

$$r_{in,e} = \frac{\Pi'_{in}}{2\pi} \tag{2.11}$$

$$\Pi_{in} = N\Pi'_{in} \tag{2.12}$$

$$\Pi_{out} = N\Pi'_{out} \tag{2.13}$$

$$d_{e,s} = \frac{4F_s}{\Pi_{out}} \tag{2.14}$$

$$F_t = \frac{N\pi \; d_{max,in} \; d_{min,in}}{4} \tag{2.15}$$

$$d_{e,t} = \frac{4F_t}{\Pi_{in}} \tag{2.16}$$

$$s = \sqrt{Fr_M \; d_{max,out} \; d_{e,s}} \tag{2.17}$$

where subscripts *in* and *out* correspond to inner and outer tube diameters and *min* and *max* correspond to minimum and maximum tube diameters.

The pressure drop on the tube side can be calculated using the following definitions.

$$f_t = 4.572Re^{-0.521}\left(\frac{d_{min,in}}{d_{max,in}}\right)^{-0.334}\left(\frac{s}{d_{e,t}}\right)^{-0.082} \tag{2.18}$$

$$\Delta P_t = f_t\left(\frac{L}{d_{e,t}}\right)\left(\frac{G_t}{F_t}\right)^2\left(\frac{1}{2\rho_t}\right) \tag{2.19}$$

The friction factor correlation is valid for $5000 \leq Re \leq 20000$.

Whereas, the pressure drop on the shell side is calculated according to:

$$f_s = 0.3164Re_s^{-0.25}(1 + 3.6Fr_M^{-0.357}) \tag{2.20}$$

for $Re_s \geq 800$ and $Fr_M \geq 100$

$$\Delta P_s = f_s\left(\frac{L}{d_{e,s}}\right)\left(\frac{G_s}{F_s}\right)^2\left(\frac{1}{2\rho_s}\right) \tag{2.21}$$

2.1.2 Heat Transfer

Thermal hydraulic correlations for plain-tube heat exchangers have been extensively studied and characterized. Presented are nondimensional forms for predicting heat

transfer. The Nusselt (Nu) is the dimensionless form of the heat transfer coefficient (h). It is dependent on the Re and Prandtl (Pr) numbers.

Plain Cylindrical Tube

For tube side flow the equations are:

$$Re_t = \frac{G_t d_{e,t}}{F_t \mu_t} \tag{2.22}$$

$$Pr_t = \frac{\mu_t (1000 * C_{p,t})}{\lambda_t} \tag{2.23}$$

There are multiple Nu correlations with different Re ranges and applications. Of most use to us is the correlation from Stefan and Preuber for laminar flow inside of a plain tube:

$$Nu = 3.657 + \frac{0.0677(RePr(d_e/L))^{1.33}}{1 + 0.1Pr(Re(d_e/L))^{0.3}} \tag{2.24}$$

This correlation is valid for: $Re \leq 2300$

Other correlations used in this work include Gnielinski:

$$Nu = \frac{\frac{f}{8}(Re - 1000)Pr}{1 + 12.7\sqrt{\frac{f}{8}}(Pr^{0.67} - 1)} * (1 + \left(\frac{d_e}{L}\right)^{0.67}) \tag{2.25}$$

where f:

$$f = (1.82 * \log_{10}(Re) - 1.64)^{-2} \tag{2.26}$$

Gnielinski is valid for $2300 \leq Re \leq 10000$. For $10000 \leq Re$ the Dittus and Boelter correlation is used:

$$Nu = 0.023 Re^{0.8} Pr^{0.4} \tag{2.27}$$

Twisted Tube

A few which we will be using are the Si (tube and shell side), Yang (tube side) and Dzyubenko (shell side)[8]. The tube side correlations are shown here.

Si:

$$Nu_t = 0.396 Re^{0.544} \left(\frac{s}{d_{e,t}}\right)^{0.161} \left(\frac{s}{d_{max,in}}\right)^{-0.519} Pr_t^{0.33} \tag{2.28}$$

This correlation is valid for $1000 \leq Re_t \leq 17000$ and $6.86 \leq (s/d_{e,t}) \leq 11.9$.

Yang:

$$Nu_t = 0.034 Re^{0.784} Pr^{0.333} \left(\frac{d_{min,in}}{d_{max,in}}\right)^{-0.590} \left(\frac{s}{d_e}\right)^{-0.165} \tag{2.29}$$

Which is valid for $5000 \leq Re_t \leq 20000$, $0.2 \leq s \leq 0.4$, $0.0198 \leq d_{max,in} \leq 0.0218$, and $0.0058 \leq d_{min,in} \leq 0.0094$

And for the shell-side Dzyubenko:

$2000 \leq Re_s \leq 30000$ and $63.6 \leq Fr_M \leq 1150$

$$Nu_s = 6.05e6 Fr_m^{-2.494+0.235 log Fr_M} Re_s^{n+a log Re_s} \left(\frac{\mu_{w,s}}{\mu_s}\right)^{-0.14} Pr^{0.4} \tag{2.30}$$

and Si:

$$Nu_s = 0.2370 Re^{0.7602} Fr_M^{-0.4347} \left(1 + 3.6 Fr_M^{-0.357}\right) Pr^{0.33} \tag{2.31}$$

for $231 \leq Fr_M \leq 392$ and $2000 \leq Re_s \leq 10000$

The heat transfer coefficient can then be calculated as:

$$h_t = Nu_t \left(\frac{\lambda_t}{d_{e,t}} \right) \tag{2.32}$$

2.1.3 Effectiveness-NTU and the LMTD Methods

For two-fluid heat exchangers, it is relatively simple to design or predict the performance of the heat exchanger using two methods, the log mean temperature difference (LMTD) and the effectiveness-NTU (ξ-NTU). The heat transfer between the hot and cold fluids in the heat exchanger can be related to the change in temperature of the fluids.

$$q = \dot{m} c_p (\Delta T) \tag{2.33}$$

As ΔT varies with position in the exchanger, it is important to use the mean temperature difference. The form of ΔT_{lm} depends on the flow configuration of the heat exchanger. For a counterflow heat exchanger:

$$\Delta T_{lm} = \frac{(T_{h,o} - T_{c,i}) - (T_{h,i} - T_{c,o})}{ln((T_{h,o} - T_{c,i})/(T_{h,i} - T_{c,o}))} \tag{2.34}$$

In defining the effectiveness of a heat exchanger, it is important to determine the maximum possible heat transfer rate q_{max} which is possible between the two fluids. A minimum heat capacity rate C_{min} must be established as the smaller of C_h or C_c where $C_{c,h}$ is $\dot{m} c_{p,(c,h)}$. The maximum possible heat transfer rate is then:

$$q_{max} = C_{min}(T_{h,i} - T_{c,i}) \tag{2.35}$$

The effectiveness ε is then defined as the ratio of the actual heat transfer to the maximum possible heat transfer or:

$$\varepsilon = \frac{q}{q_{max}} \tag{2.36}$$

Given the effectiveness of a heat exchanger, the actual heat transfer rate of any fluid combination can be determined from:

$$q = \varepsilon C_{min}(T_{h,i} - T_{c,i}) \tag{2.37}$$

A parameter which is necessary for this method is the number of transfer units or NTU which is defined as:

$$NTU = \frac{UA}{C_{min}} \tag{2.38}$$

There is a relationship between the effectiveness and NTU based on the geometry of the heat exchanger. These relationships can be found in tables or books [11]. For a counterflow heat exchanger:

$$\varepsilon = \frac{1 - exp[-NTU(1 - C_r)]}{1 - C_r exp[-NTU(1 - C_r)]} \qquad where \qquad C_r = \frac{C_{min}}{C_{max}} \tag{2.39}$$

2.2 Three-Fluid Heat Exchanger Theory

Three-fluid heat exchangers are used in many applications including food processing, cryogenic and the petrochemical industry. Three fluids however pose a significantly more complex problem in terms of predicting heat transfer performance and defining the effectiveness of the heat exchanger. Three fluid heat exchangers are classified ac-

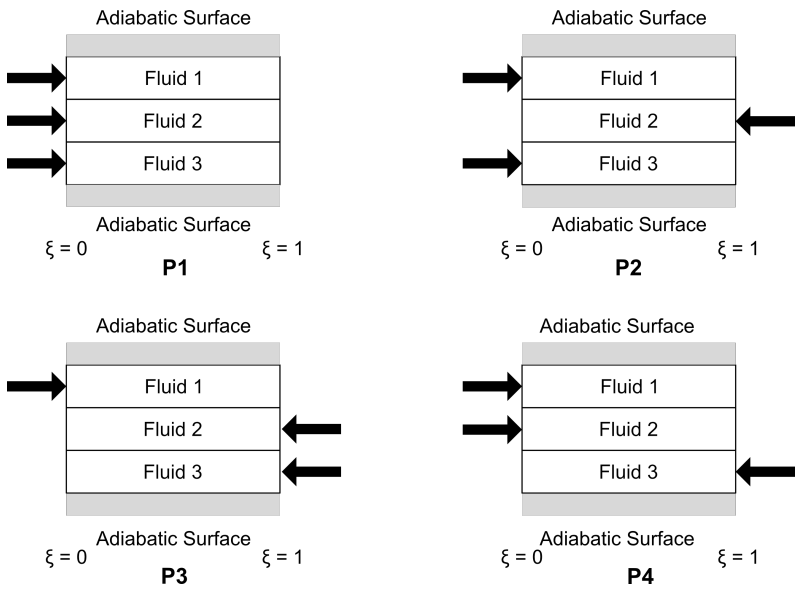

Figure 2.1: Flow directions corresponding to the boundary conditions defined in Table 2.1

cording to their flow configuration and construction, including the number of thermal communications:

- One fluid stream transfers heat to other fluid streams (two thermal communications)

- All fluids transfer heat among each other (three thermal communications)

The focus of this work will be on tubular heat exchangers with two thermal communications. Figure 2.1 depicts the flow arrangements of parallel stream three-fluid heat exchangers. During initial mathematical modeling it was determined for our purposes that flow arrangement P3 would be the most effective. This modeling will be discussed in Chapter 4.

2.2.1 Heat Transfer

Three-fluid heat exchanger design and analysis relies on the use of five dimensionless independent parameters:

- $NTU = \frac{(UA)_{1,2}}{(\dot{m}c_p)_1}$
- $C^*_{1,2} = \frac{(\dot{m}c_p)_1}{(\dot{m}c_p)_2}$
- $C^*_{3,2} = \frac{(\dot{m}c_p)_3}{(\dot{m}c_p)_2}$
- $R^* = \frac{(UA)_{3,2}}{(UA)_{1,2}}$
- $\Theta_{3,in} = \frac{T_{3,in} - T_{1,in}}{T_{2,in} - T_{1,in}}$

As described in Sekulic and Shah [12], the effectiveness-NTU approach is well known for two-fluid heat exchangers but can be extended for three-fluid heat exchangers. This process is described here. It is important to note that there are many idealizations that are adopted for this method to be accurate. They are described here:

1. The heat exchanger operates under steady state conditions
2. Heat losses to the surroundings are negligible; the heat exchanger is adiabatic
3. Fluid properties, including specific heats, are constant
4. There are no internal heat sources or sinks
5. In parallel stream heat exchangers, there is no temperature gradient normal to flow direction
6. Only one fluid transfers heat with the other two fluids
7. The fluids do not change phase within the heat exchanger

8. There is no heat conduction in the fluids or walls parallel to the fluid flow direction

9. Velocity and axial temperature profiles are uniform within the fluids

10. The heat transfer area is uniformly distributed on each fluid side

Table 2.1 depicts the energy balances of a parallel stream three-fluid heat exchanger. The governing energy equations are obtained from the energy balance within the heat exchanger. This balance is described here:

$$i_1 \left[\dot{m}c_p T - \dot{m}c_p \left(T + \frac{dT}{dA} dA \right) \right]_1 + (UdA)_{1,2}(T_2 - T_1) = 0 \tag{2.40a}$$

$$i_2 \left[\dot{m}c_p T - \dot{m}c_p \left(T + \frac{dT}{dA} dA \right) \right]_2 - (UdA)_{1,2}(T_2 - T_1) - (UdA)_{3,2}(T_2 - T_3) = 0 \tag{2.40b}$$

$$i_3 \left[\dot{m}c_p T - \dot{m}c_p \left(T + \frac{dT}{dA} dA \right) \right]_3 + (UdA)_{3,2}(T_2 - T_3) = 0 \tag{2.40c}$$

$i = +1$ or -1 for each fluid depending on the flow direction. The governing equations are algebraically simplified and nondimensionalized respectively in the following sets of equations.

$$\frac{dT_1}{dx} + \frac{(UA)_{1,2}}{(\dot{m}c_p)_1}(T_1 - T_2) = 0 \tag{2.41a}$$

$$i_2 \frac{dT_2}{dx} + \frac{(UA)_{1,2}}{(\dot{m}c_p)_2}(T_2 - T_1) + \frac{(UA)_{3,2}}{(\dot{m}c_p)_2}(T_2 - T_3) = 0 \tag{2.41b}$$

$$i_3 \frac{dT_3}{dx} + \frac{(UA)_{3,2}}{(\dot{m}c_p)_3}(T_3 - T_2) = 0 \tag{2.41c}$$

It is important to note that we assume $i_1 = +1$ and as such it is omitted from

Table 2.1: Boundary conditions defined for parallel stream couplings

	P1	P1	P2	P2	P3	P3	P4	P4
j	ξ	Θ	ξ	Θ	ξ	Θ	ξ	Θ
1	0	0	0	0	0	0	0	0
2	0	1	1	1	1	1	0	1
3	0	$\Theta_{3,in}$	0	$\Theta_{3,in}$	0	$\Theta_{3,in}$	0	$\Theta_{3,in}$

further equations. These simplified equations can be nondimensionalized and are shown here:

$$\frac{d\Theta_1}{d\xi} = NTU_1(\Theta_2 - \Theta_1) \tag{2.42a}$$

$$i_2\frac{d\Theta_2}{d\xi} = C^*_{1,2}NTU_1(\Theta_1 - \Theta_2) + C^*_{1,2}R^*NTU_1(\Theta_3 - \Theta_2) \tag{2.42b}$$

$$i_3\frac{d\Theta_3}{d\xi} = \frac{C^*_{1,2}}{C^*_{3,2}}R^*NTU_1(\Theta_2 - \Theta_3) \tag{2.42c}$$

Table 2.1 describes the boundary conditions which can be applied to the dimensionless equations above based on the the fluid stream arrangement.

The explicit analytical solution of this set of differential equations can be found by utilizing Laplace transforms. The dimensionless temperature distributions are given by:

$$\Theta_j(\xi) = \Theta_{2,\xi=0}\,\Phi_j(\xi) + \Theta_{3,\xi=0}\,\Psi_j(\xi) \qquad for \quad j = 1,2,3 \tag{2.43}$$

The functions $\Phi_j(\xi)$ and $\Psi_j(\xi)$ can be found in Table 2.2.

The following equations define the rest of the variables used in Table 2.2

$$E^+(\xi) = e^{s_1\xi} + e^{s_2\xi} \tag{2.44a}$$

Table 2.2: Definitions of $\Phi_j(\xi)$ and $\Psi_j(\xi)$ based on fluid stream

j	$\Phi_j(\xi)$	$\Psi_j(\xi)$
1	$i_2 i_3 \frac{1}{C^*_{3,2}}\Psi_1(\xi) + \frac{1}{\gamma}E^-(\xi)$	$\frac{1}{2\alpha}(2 - E^+(\xi) - \frac{\beta}{\gamma}E^-(\xi))$
2	$i_2 i_3 \frac{1}{C^*_{3,2}}\Psi_2(\xi) + \frac{1}{2}(E^+(\xi) - \frac{\beta-2}{\gamma}E^-(\xi))$	$\Psi_1(\xi) + i_2\frac{R^*C^*_{1,2}}{\gamma}E^-(\xi)$
3	$i_3\frac{1}{C^*_{3,2}}(i_2(1-\Phi_2(\xi)) - C^*_{1,2}\Phi_1(\xi)$	$1 - i_3\frac{1}{C^*_{3,2}}i_2\Psi_2(\xi) + C^*_{1,2}\Psi_1(\xi)$

$$E^-(\xi) = e^{s_1\xi} - e^{s_2\xi} \tag{2.44b}$$

$$s_1 = -(\beta - \gamma)\frac{NTU_1}{2} \tag{2.44c}$$

$$s_2 = -(\beta + \gamma)\frac{NTU_1}{2} \tag{2.44d}$$

$$\alpha = 1 + i_3\frac{1}{C^*_{3,2}}(i_2 + C^*_{1,2}) \tag{2.44e}$$

$$\beta = 1 + i_2 C^*_{1,2}\left(1 + R^*\left(1 + i_2 i_3\frac{1}{C^*_{3,2}}\right)\right) \tag{2.44f}$$

$$\gamma = (\beta^2 - 4i_2 R^* C^*_{1,2}\alpha)^{\frac{1}{2}} \tag{2.44g}$$

Table 2.2 defines the values of $\Phi_j(\xi)$ and $\Psi_j(\xi)$. These equations can be used to calculate temperature profiles and exit temperatures for fluids based on flow configurations.

2.2.2 Defining Effectiveness

The effectiveness of a two-fluid heat exchanger is a well-defined metric which provides information on the performance the heat exchanger and can be compared to any other two-fluid heat exchanger. It can be defined as $\frac{Q}{Q_{max}}$ where Q_{max} is the

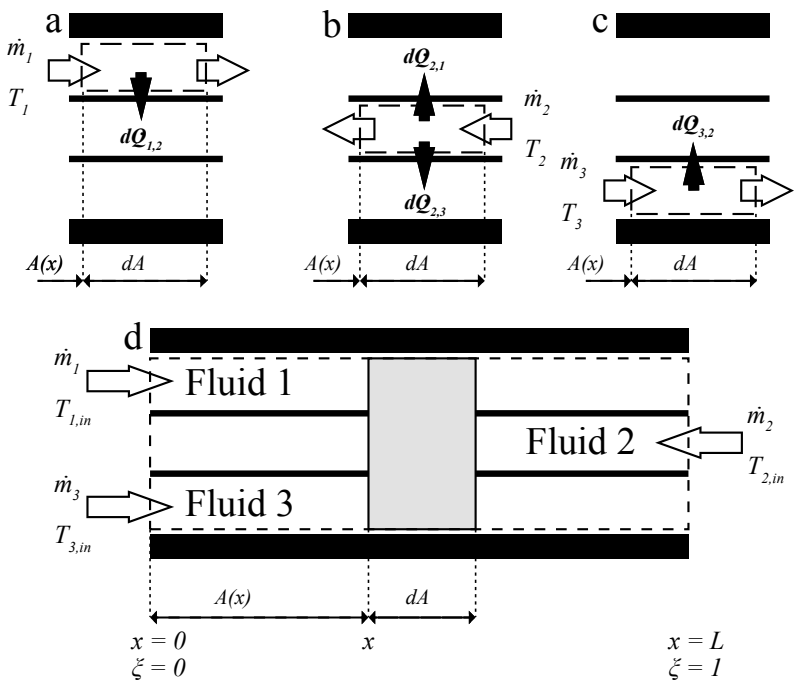

Figure 2.2: The balance of energy in a differential area of a three-fluid counterflow heat exchanger

maximum possible heat transfer rate given a heat exchanger of infinite length for a given geometry and Q is the achieved heat transfer rate. This definition does not work well for a three-fluid heat exchanger as heat can be transferred in many different possibilities. There is no universally accepted definition for defining three-fluid heat exchanger effectiveness. In defining the effectiveness of the exchanger, it is important to define the purpose of the heat exchanger. Two heat exchangers could be of the same geometry and have the same effectiveness however, they could have drastically different purposes resulting in different goals for the heat exchanger fluids.

This work attempts to simulate the idea of a heat exchanger for the FHR. Early concepts of a shell-and-tube heat exchanger design place flibe as the hot shell-side fluid with the cooler fluid(s) on the tube-side of the exchanger. A hot, shell-side fluid is used to heat a cool, tube-side fluid via an intermediate fluid. Thus, we determine

the purpose of the exchanger to heat the tube-side fluid or fluid three. We judge the performance of each heat exchanger and flow configuration on their ability to heat fluid three.

There are multiple effectivenesses which are useful for analyzing the performance of a 3FHE. The first is the overall effectiveness, which is defined similarly to its two-fluid heat exchanger counterpart as:

$$\varepsilon_{3FHE} = \frac{Actual\ heat\ transfer\ rate}{Maximum\ possible\ heat\ transfer\ rate} \tag{2.45}$$

or

$$\varepsilon_{3FHE} = \frac{\dot{Q}_{actual}}{\dot{Q}_{max}} \tag{2.46}$$

The effectiveness is a function of five parameters just as the temperature distributions are. That is:

$$\varepsilon_{3FHE} = \varepsilon(NTU_1, C^*_{1,2}, C^*_{3,2}, R^*, \Theta_{3,in}, Flow\ arrangement) \tag{2.47}$$

Sekulic and Shah assume that fluid two has the highest inlet temperature. This is not the case for this work, fluid 1 has the highest inlet temperature. The overall effectiveness of the heat exchanger is therefore defined qualitatively as the ratio of the actual cooling of fluid one to the maximum possible cooling of fluid one. Expressed quantitatively, that is:

$$\varepsilon_{3FHE} = \frac{C^*_{2,1}(\Theta_{2,out} - \Theta_{2,in}) + C^*_{3,1}\Theta_{3,out}}{C^*_{2,1}(1 - \Theta_{2,in}) + C^*_{3,1}} \tag{2.48}$$

For the case of the 3FHE, it is not enough to define the overall effectiveness. As in the name, this effectiveness provides information for the combined effects of the changing enthalpy levels of all three fluids. It is therefore important to define a

so-called temperature effectiveness for the auxiliary fluids in reference to the purpose fluid. These temperature effectivenesses are as follows:

$$\vartheta_3 = \Theta_{3,out} \tag{2.49}$$

and

$$\vartheta_2 = \frac{\Theta_{2,out} - \Theta_{2,in}}{\Theta_{1,in} - \Theta_{2,in}} \tag{2.50}$$

These two values provide information as to the degree which each auxiliary fluid approached the inlet temperature of the purpose fluid (fluid one). It is important to note that the temperature effectiveness is not a figure of merit but an indicator of the temperature change.

Chapter 3

Heat Transfer Enhancement due to Twisted-Tubes

The main focus of the thermal fluids laboratory at the University of New Mexico (UNM) has been to perform thermal hydraulics experiments with the intent to provide validation data for predictive tools. The laboratory began to collect data on the performance of a twisted tube heat exchanger early in 2017[8]. The purpose of this experiment was to provide validation data for the twisted tube heat exchanger and to quantify the enhancement of the twisted tubes over the plain tube counterpart. As such, experiments regarding the twisted tube heat exchanger were performed by Joel Hughes and are presented as a part of his dissertation [8]. Dr. Hughes tested the twisted tube heat exchanger under buoyant and forced convection flow simulating FHR conditions. He tested the accuracy of multiple equations for predicting heat transfer in twisted tubes and ultimately created his own based on these equations to better match the data. The experimental conditions will be shown here as they have been repeated to test the plain tube heat exchanger for comparison to the twisted tube heat exchanger. It is important to note that much of this chapter will be a summary of Hughes' work. The work performed by the author is an important ad-

dition to Hughes' work and provides baseline heat transfer results for the plain-tube heat exchanger.

3.1 Scaling for Heat Transfer

Bardet and Forsberg [13] discovered that the non-dimensional numbers, which are used for predicting heat transfer, in the FHR could be scaled using simulant fluids which are like that of mineral oil. Scaled experiments have been used throughout the nuclear industry as they allow information to be learned about nuclear systems without needing to construct and pay for full scale systems. This saves the industry time and money while providing valuable data. There are multiple facilities which have been built solely for scaled experiments for the FHR. The University of California, Berkeley has constructed both the Pebble Scaled High Temperature Heat Transfer ($PS - HT^2$) facility and the Compact Integral Effects Test (CIET) facility. These facilities both operate with the DOWTHERM A heat transfer fluid.

The Reynolds, Froude, Grashof, and Prandtl numbers are the numbers which are of importance in heat transfer scaling. The Prandtl number can be scaled solely with the thermo-physical properties of the fluids. As seen in figure 1.3, the Prandtl number changes similarly to flibe at significantly reduced temperatures.

The Reynolds, Froude, and Grashof numbers are matched by imposing certain length and temperature scale restrictions. These are:

$$\left(\frac{L_{mod}}{L_{prot}}\right)^{3/2} = \left(\frac{\nu_{mod}}{\nu_{prot}}\right) \tag{3.1}$$

$$\left(\frac{\beta_{mod}}{\beta_{prot}}\right) = \left(\frac{\Delta T_{prot}}{\Delta T_{mod}}\right) \tag{3.2}$$

where the subscripts *mod* and *prot* refer to the model (reduced scale) and prototype (full scale).

With scaled heat transfer experiments, there are notable distortions. For this experiment, the most notable is the effect of radiation heat transfer. In the scaled experiment, temperatures are not nearly high enough to invoke significant transfer of heat by radiation. As such, it is important for design concepts based on these numbers to err conservatively.

3.2 Heat Transfer Facility (HTF)

The heat transfer facility (HTF) at UNM is a facility designed to perform reduced-scale heat transfer experiments on prototype heat exchanger designs for advanced reactor concepts. Data from the facility is intended to fulfill two goals: to explore heat exchanger performance in the space of conditions relevant to the FHR and to validate thermal-hydraulics tools used to predict heat transfer performance. This work focuses on the former goal while providing experimental data to other groups and institutions for use in validating their tools.

Initially, the facility was built as two closed flow loops for circulating either water or simulant fluid DOWTHERM A. Since this twisted tube test, the facility has undergone modifications in order to test a concept double-wall heat exchanger. These modifications will be discussed in the next chapter and the "base" facility will be discussed here.

The facility uses a custom-built electrical resistance heater to deposit up to $5 - 6kW_{th}$ in the primary loop. The power supply to the heater is controlled through the data acquisition system utilizing a proportional integral derivative (PID) controller. This type of controller is commonly used in feedback loop systems to reach and

maintain steady state configuration. This loop uses a Coriolis flow meter for high accuracy of volumetric flow rate especially under natural circulation conditions. The primary loop functions as the shell-side fluid of the test section heat exchanger. The test section heat exchanger is either the aforementioned plain-tube or twisted-tube dip-type shell-and-tube heat exchanger. This loop also features a small tube and valve array which can change the direction of this loop to either up-flow or down-flow based on the direction through the test section. This array is also used to bypass the pump in order to reduce loop resistance during natural circulation tests. A graphic of this loop can be seen in figure 3.1.

Like the primary loop, the secondary loop can be filled with water or DOWTHERM A. For these tests, both loops were filled with DOWTHERM A. The secondary loop functions as the tube-side fluid in the test section. The loop can force fluid flow in the loop over 10 gpm and can be throttled with valves down to 1.5 gpm. The fluid is heated in the test section and is subsequently cooled by a heat exchanger connected to chilled water as the heat sink. A graphic of this loop can be seen in figure 3.2.

The chilled water supply initially was controlled by a chiller. The chiller turns on when the temperature of the water reaches a set-point and turns off after it has been chilled. This on and off action led to a "sawtooth" function within the chilled water which led to a large uncertainty within the data as the function cycled approximately every 20 minutes. Eventually, the chiller was bypassed and the heat exchanger was directly connected to the building's chilled water supply. While this reduced uncertainty from the sawtooth of the chiller, fluctuations in the supply are also a cause of uncertainty.

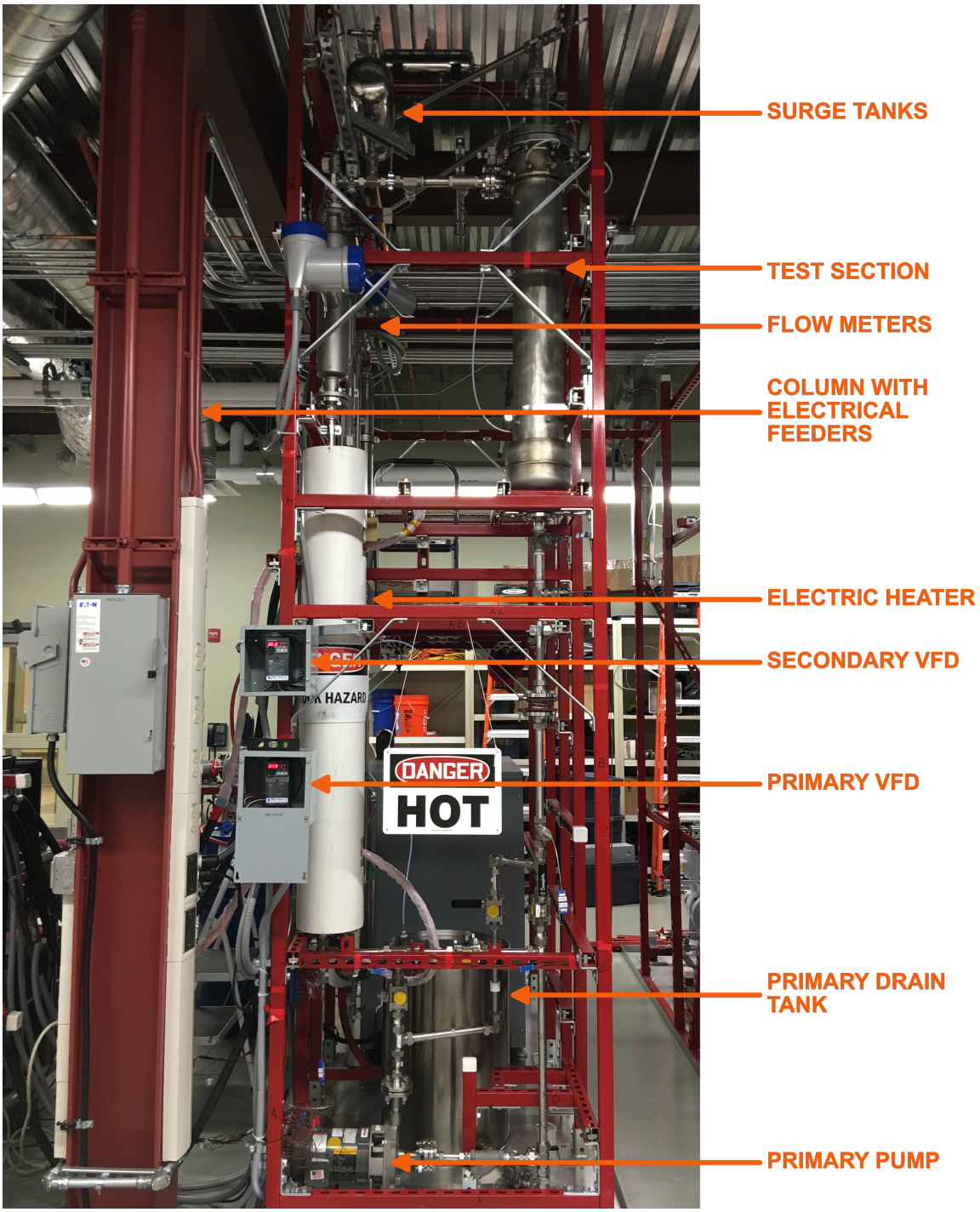

Figure 3.1: The primary loop of the HTF with labels

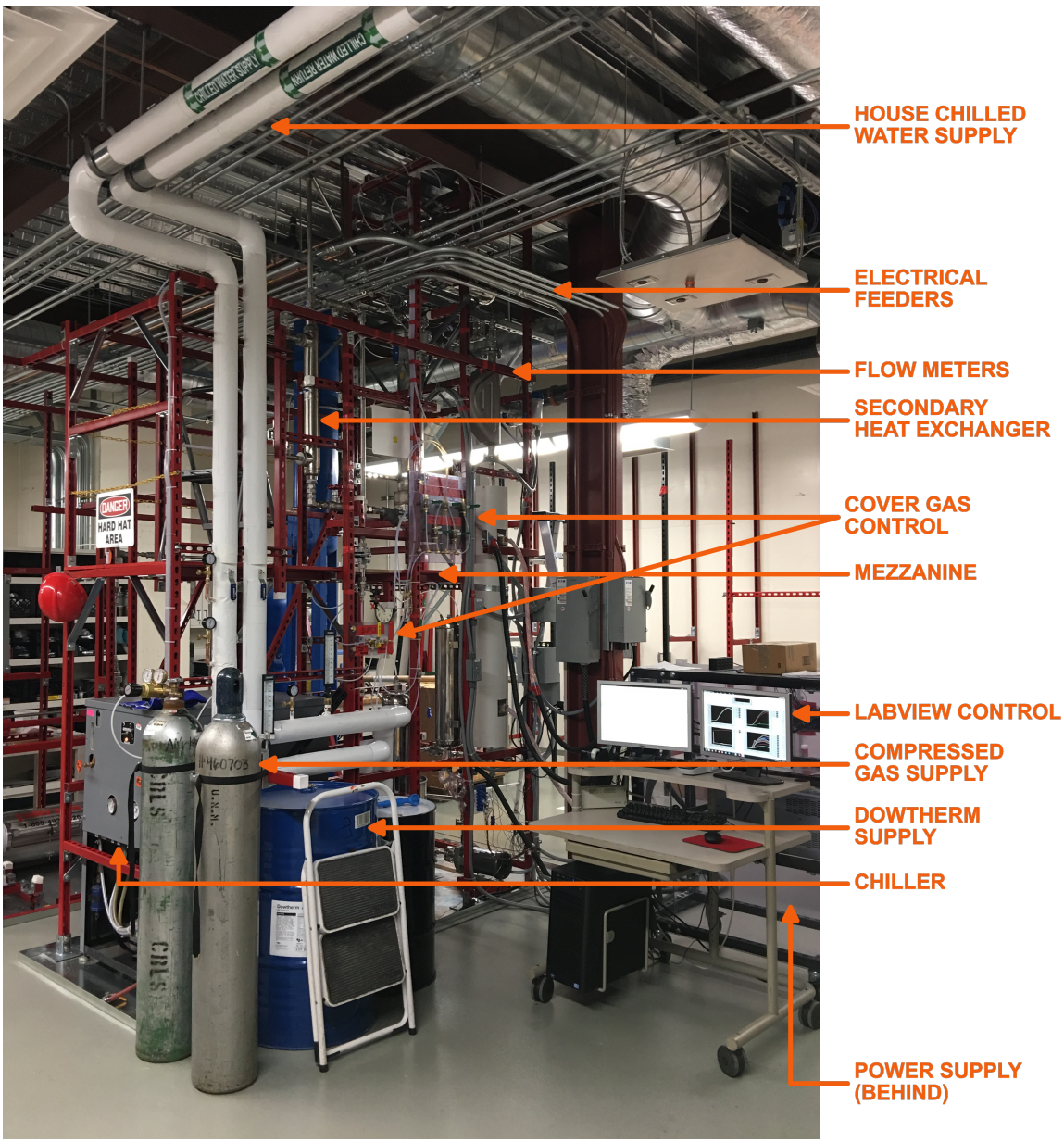

Figure 3.2: The secondary loop of the HTF with labels

3.3 Experimental Design

The function of the experiment is to test plain and twisted tube heat exchangers under conditions relevant to the FHR. Based on the scaling properties addressed

above, the heat exchangers were tested under multiple conditions to explore the space of normal operation and possible emergency scenarios. Under buoyancy-driven flow, the average test section temperature contained a range from $60°C - 110°C$. Larger temperature gradients result in larger fluid Reynolds numbers (40 - 200). Similarly for forced convective flow, test section average temperatures were varied through a similar range. The force due to the loop pumps however gave a wide range of Reynolds numbers ($\sim 60 - 1200$) to test through.

3.4 Data Reduction

Typical heat exchanger analysis determines heat transfer coefficients by forcing either a constant temperature or constant heat flux for one side of the heat exchanger. Typically, testing is done by boiling water on one side of the heat exchanger. In cases where this is not possible, or a two-stream heat exchanger, the individual heat transfer coefficients can be backed out by the overall heat transfer coefficient. One side of the heat exchanger is denoted as the "target" side and the other is the "non-target" side. The target heat transfer coefficient's value is the goal of the analysis and the non-target heat transfer coefficient is estimated using available correlations. The non-target heat transfer coefficient is maximized to reduce its contribution to the uncertainty in the target heat transfer coefficient. This method is expanded on by Hughes.

It is important to note that each of the heat exchangers are identical except for the twisted or plain tubes. As shown in Figure 3.3, the heat exchangers are dip-type shell-and-tube heat exchangers with a central downcomer and two plena. The tube-side flow is therefore complex as the fluid inlet travels the length of the central downcomer to a lower plenum and is distributed to the tubes. The tube-side fluid then collects in an upper plenum and exits the heat exchanger. The complexity of

Figure 3.3: A masked photo of the two dip-type heat exchangers side-by-side

the analysis is therefore increased as the exchanger is no longer counterflow or co-currentflow but is a combination of the two. The geometry of the heat exchanger also provides multiple parallel heat transfer pathways which are of unequal size and thus make calculating the overall thermal resistance of the heat exchanger more difficult.

The chosen subscripts in following thermal resistance theory have the following definitions:

1. *tot*:total heat exchanger
2. *o*:overall
3. *s*:shell-side
4. *t*:tube-side

5. *w*:wall

6. *tubes*:tube bundle

7. *dc*:downcomer

8. *p-sides*:plena sides

9. *p-ends*:plena ends

where the plena were split due to their difference in geometry. The total thermal resistance for the heat exchanger can be expressed as:

$$\frac{1}{R_{o,tot}} = \frac{1}{R_{o,tubes}} + \frac{1}{R_{o,dc}} + \frac{1}{R_{o,p-sides}} + \frac{1}{R_{o,p-ends}} \tag{3.3}$$

where the overall resistances are a summation of the corresponding individual resistances:

$$R_{o,tubes} = R_{s,tubes} + R_{w,tubes} + R_{t,tubes} \tag{3.4a}$$

$$R_{o,dc} = R_{s,dc} + R_{w,dc} + R_{t,dc} \tag{3.4b}$$

$$R_{o,p-sides} = R_{s,p-sides} + R_{w,p-sides} + R_{t,p-sides} \tag{3.4c}$$

$$R_{o,p-ends} = R_{s,p-ends} + R_{w,p-ends} + R_{t,p-ends} \tag{3.4d}$$

The individual thermal resistances including the twisted tube walls can be found in Hughes' work.

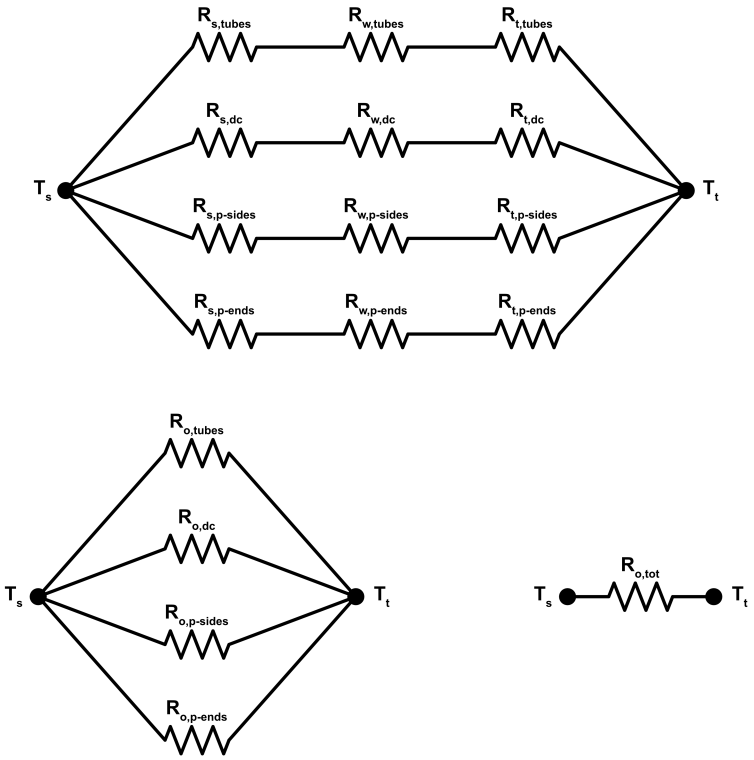

Figure 3.4: Simplifications of the thermal circuit

3.5 Results

The results of the heat transfer experiments of the two heat exchangers are divided into sections based on the flow regime: forced convection and natural and mixed convection. This section will also review the results for the twisted tube heat exchanger which can be found in Dr. Hughes' dissertation [8]. As for new data, the results for the plain tube experiment will be presented along with a comparison of the results for the ultimate conclusion on the increase in heat transfer performance due to the twisted tubes.

For twisted tube heat exchangers, the shell-side correlations follow the general form:

$$Nu_F = f(Re, Pr, (T_w/T_f), Fr_M) \tag{3.5}$$

where the modified Froude number (Fr_M) is a measure of the twisted tube geometry and (T_w/T_f) is a viscosity correction factor typically used for gases. Of available correlations, Hughes found that not many addressed the Re ranges which are used here. Figure 3.5 shows the available Nu correlations and the ranges which they are valid in. It is important to note that these correlations are only valid in certain Fr_M ranges. These correlations are depicted in Hughes[8] and are repeated here in Figure 3.6.

Summarizing Hughes' work, it was found that most correlations for Nu left much to be desired. Hughes uses mean absolute relative error (MARE) and maximum absolute relative error (MaxRE) to determine the agreement between the data taken and each correlation.

Experimental testing of the twisted tube heat exchanger was used not only for specific heat transfer tests but also for exploratory testing of the facility's capabilities. As such, there are a significant number of duplicate points for each Re number when compared to the plain tube data. In reducing resources used by the facility, it was deemed that tests for each Re number did not need to be duplicated for the plain tube heat exchanger. After testing the twisted tube heat exchanger, the test matrix for the plain tube heat exchanger attempted to cover the range of Re numbers tested by the twisted tube heat exchanger.

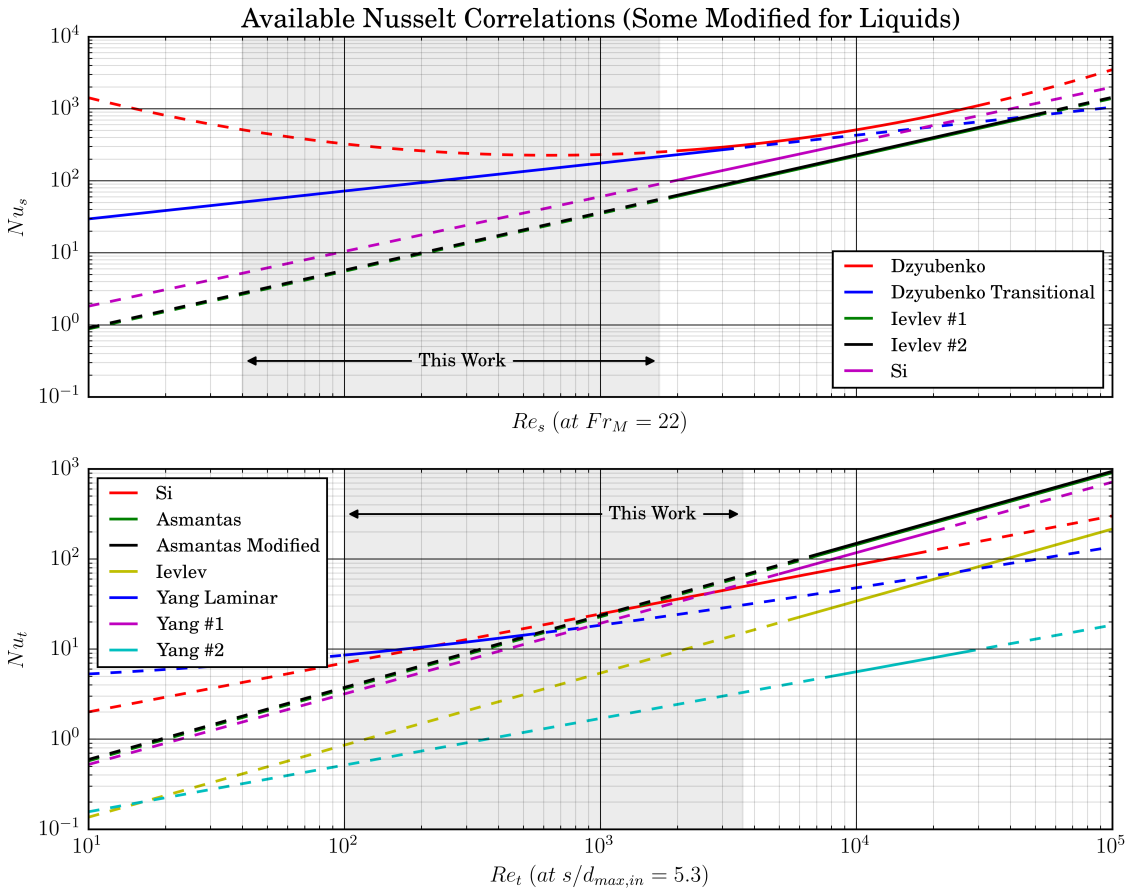

Figure 3.5: Comparison of available correlations based on Re validity

3.5.1 Natural Circulation

The HTF has the ability to run in multiple different flow configurations. The key to changing configurations in the facility is the array of ball valves shown at the bottom of Figure 3.7. These valves not only control the flow direction through the test section but they are used to bypass the primary pump to reduce the system resistance. These valves are also used to reduce flow rate under natural circulation conditions to allow for lower flow rates at higher temperature set points.

Figure 3.8 plots both the calculated Nusselt number for the twisted tube heat

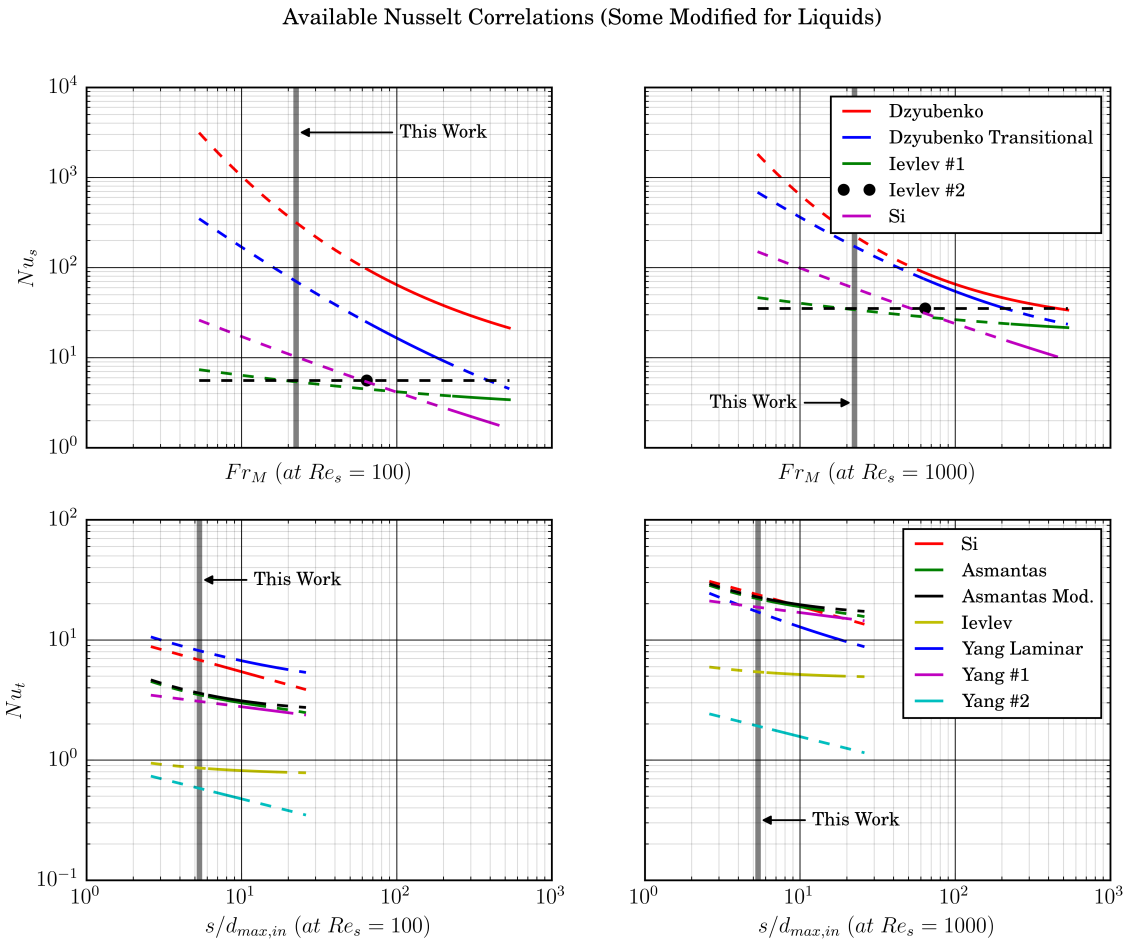

Figure 3.6: Comparison of available correlations based on Fr_M

exchanger as well as the predicted Nusselt number according to Hughes' developed correlation. The next figure, Figure 3.9, shows the plain tube heat exchanger's calculated Nusselt number alongside the fit for the data using an exponential function. The plain tube fit and the Hughes correlation are used in determining the percent improvement in the twisted tube heat exchanger over the plain tube heat exchanger.

Figure 3.10 shows the comparison of the $\frac{Nu}{Pr^{0.4}}$ in the twisted tube heat exchanger vs. its plain tube counterpart. The $\frac{Nu}{Pr^{0.4}}$ was chosen to reduce the variance between the data points while still maintaining the general trend based on the Re number.

Figure 3.11 describes the percent improvement in Nu number based on the Re number in the twisted tube heat exchanger over the Re number. As mentioned, the percent improvement value was determined over the range of Re numbers by evaluating the Hughes correlation for the twisted tube heat exchanger and plain tube fitting at the Re value and subtracting the fitting from the correlation. That number was then divided by the fitting value and multiplied by 100 to get the improvement as a percentage of the plain tube value. The percent improvement calculation is shown in equation 3.6.

$$\frac{Hughes\ Correlation\ Value - Plain\ Tube\ Fitting\ Value}{Plain\ Tube\ Fitting\ Value} * 100 \tag{3.6}$$

3.5.2 Forced Circulation - Up Flow

The up flow forced circulation configuration describes the flow of the primary fluid through the test section. In this configuration, The data for this configuration is presented in the same form as the previous section. Figures 3.12-3.14 show the comparison between the two heat exchangers in calculated Nu number, the fitting of the plain tube data, and the percent improvement in the twisted tube heat exchanger over the plain tube.

3.5.3 Forced Circulation - Down Flow

Again, the naming convention describes the direction of the primary fluid flow. In this configuration, the primary fluid is flowing in counterflow with the fluid flowing within the tubes of the dip-type test section heat exchanger. Figures 3.15 - 3.17 show the results for these tests.

3.6 Discussion and Conclusion

It is clear from the figures presented that the twisted tube heat exchanger provides a greater heat transfer coefficient for the shell side fluid in all shown configurations. As mentioned previously, this heat exchanger is intended to be used as the DHX and as such, will likely function under buoyancy driven flow. It is therefore important to closely examine this data set. The enhancement in heat transfer coefficient is significant in this regime, ranging from a 10-50 percent increase. The percent increase follows an odd curve, peaking around $Re = 120$ at 55% increase. The upper bound of Re numbers for the natural circulation tests approximately meets the lower bound of the forced circulation tests in the up flow direction. It appears that the percent improvement is approximately the same for Re number regardless of whether the primary fluid's movement is due to buoyancy effects or the force of a pump.

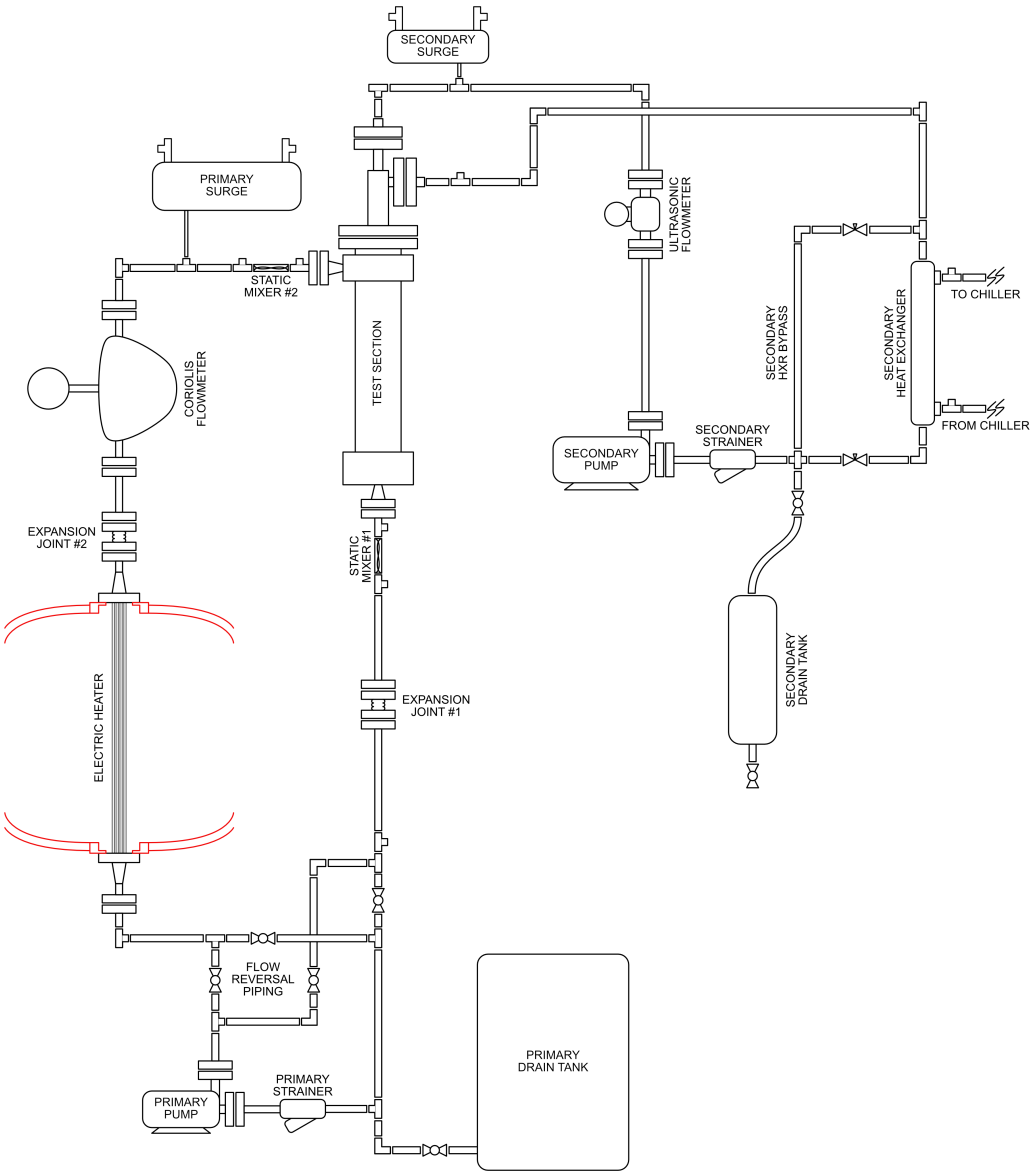

Figure 3.7: Graphic depicting the HTF, note the flow reversal piping used to control flow direction

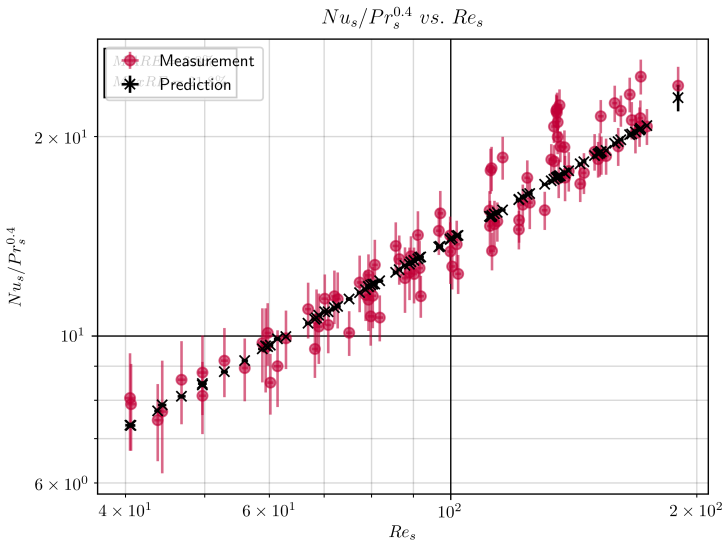

Figure 3.8: Calculated shell-side Nusselt number compared to predicted values using Hughes' developed correlation

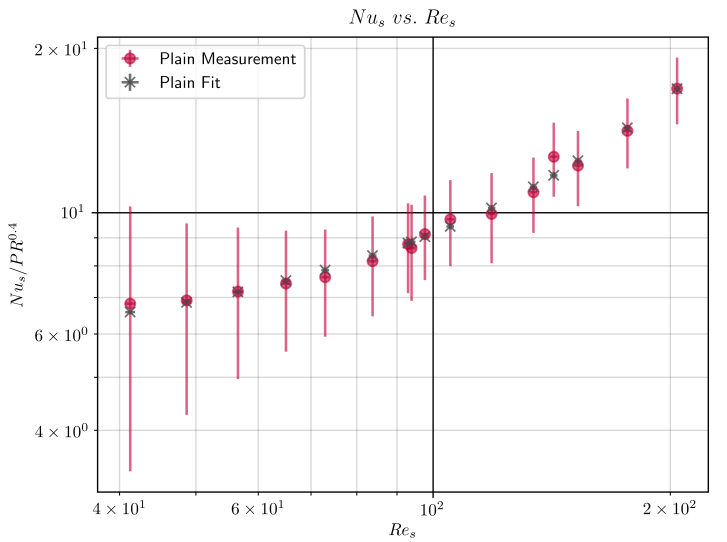

Figure 3.9: Calculated shell-side Nusselt number compared to fit of data using an exponential function

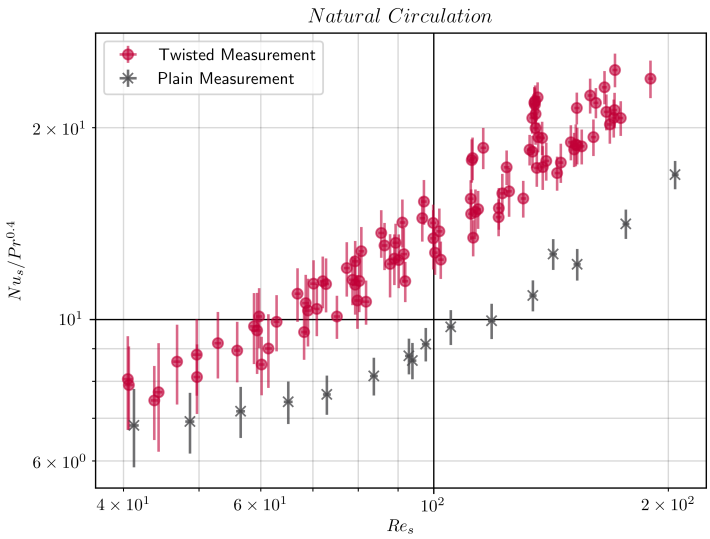

Figure 3.10: A comparison of the $\frac{Nu}{Pr^{0.4}}$ of the twisted tube heat exchanger compared to the plain tube heat exchanger

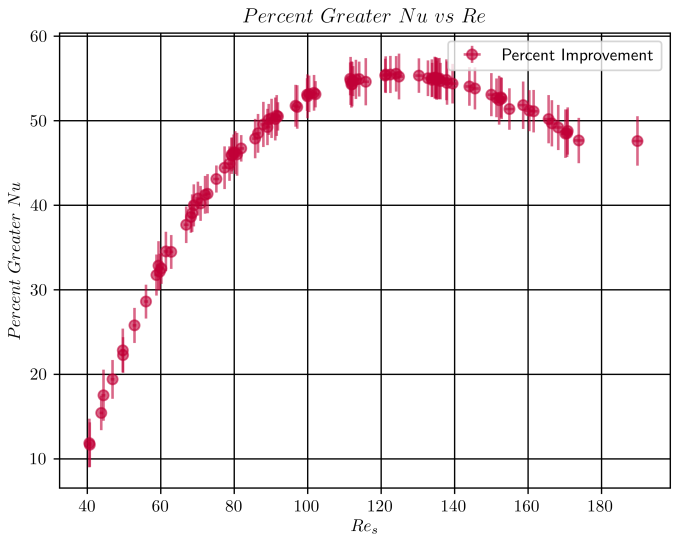

Figure 3.11: The percent improvement in $\frac{Nu}{Pr^{0.4}}$ of the twisted tube heat exchanger compared to the plain tube heat exchanger

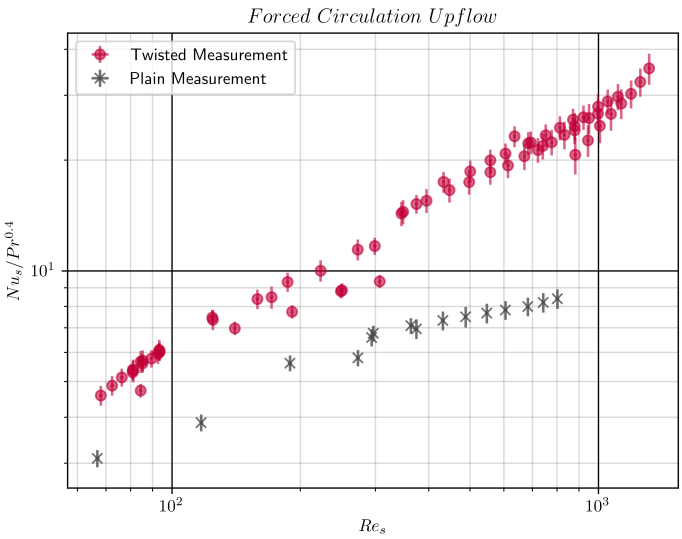

Figure 3.12: Comparison between twisted and plain tube data in forced circulation up flow configuration

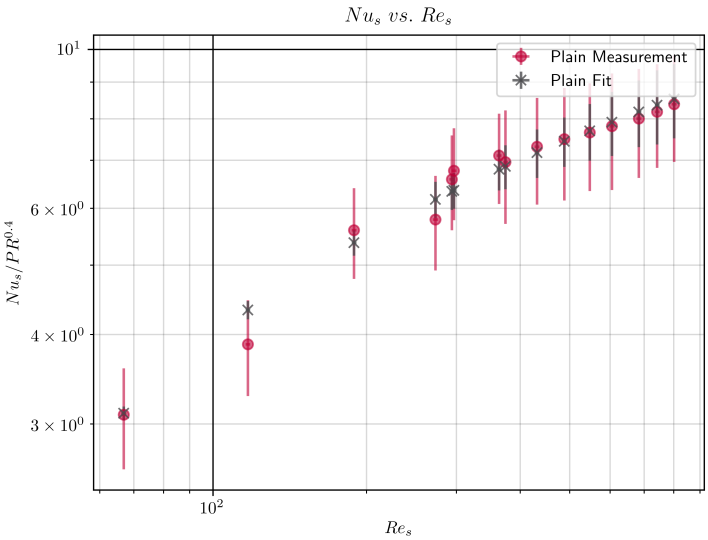

Figure 3.13: Fit to plain tube data for comparison purposes in the forced circulation up flow configuration

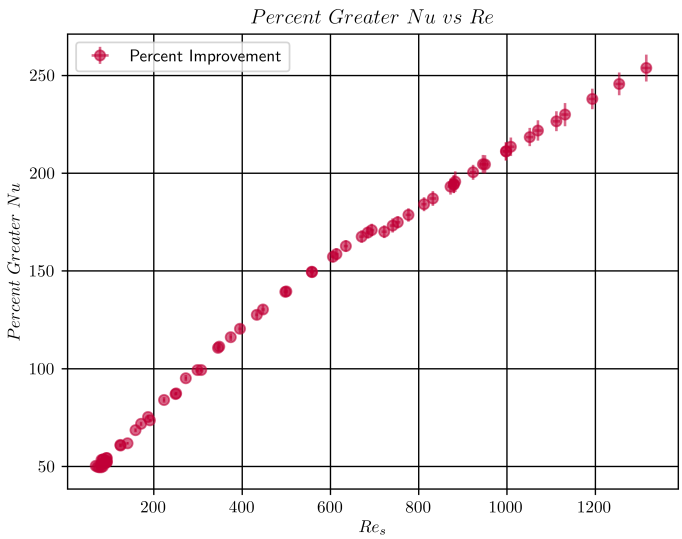

Figure 3.14: Percent improvement of the twisted tube heat exchanger compared to the plain tube heat exchanger in the forced circulation up flow configuration

Chapter 4

Single-assembly Double-wall Heat Exchanger Analysis

A possible use for the twisted-tube heat exchanger design could be as the SHX. The problem of tritium permeation, outlined above, requires some form of mitigation. Double-wall heat exchangers may play a role in the solution to this problem. It is therefore important to measure how much of an impact a double-wall heat exchanger may have on the thermal efficiency of the plant. UNM has acquired a tube-in-tube heat exchanger which has been denoted as a single-assembly double-wall heat exchanger. The heat exchanger contains a shell, annular tube, and inner tube. This experiment aims to measure the performance of the specific heat exchanger to make connections to a multiple-assembly double-wall heat exchanger. In continuing the efforts of the laboratory to quantify the effects twisted-tubes have on heat transfer performance, this experiment has acquired both a plain and twisted annular tube to test with.

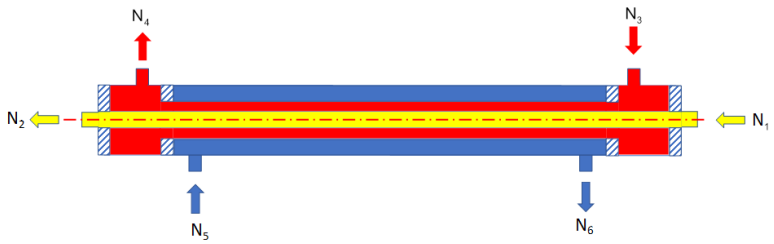

Figure 4.1: A graphic depicting the flow of the three streams within the single assembly heat exchanger

4.1 HTF Updates

As the HTF was designed for testing dip-type shell-and-tube heat exchangers, the facility needed to undergo a few changes in order to be able to test the single-assembly double-wall heat exchangers. Multiple factors were taken into account when designing the modifications including cost, ease of construction, and available laboratory space. Accommodating for the length of the heat exchanger ($\sim$ 10 feet long), and the available space in the lab, it was decided that the single-assembly heat exchanger would essentially replace the heat exchanger connecting the secondary loop to the chilled water supply. The laboratory has more vertical than horizontal space and as such, the single-assembly heat exchanger was placed vertically in an open section of the laboratory support systems.

For data acquisition, a flow meter and globe valve were installed on the chilled water supply, two globe valves and flow meters were installed for the annular fluid (one each for the air and water supply), and multiple thermocouples and pressure transducers were installed as well.

The shell-side fluid for the single-assembly heat exchanger is the DOWTHERM A in the secondary loop of the facility. The intermediate fluid can be air or water depending on the test. These fluids are once-through relying on building supplied

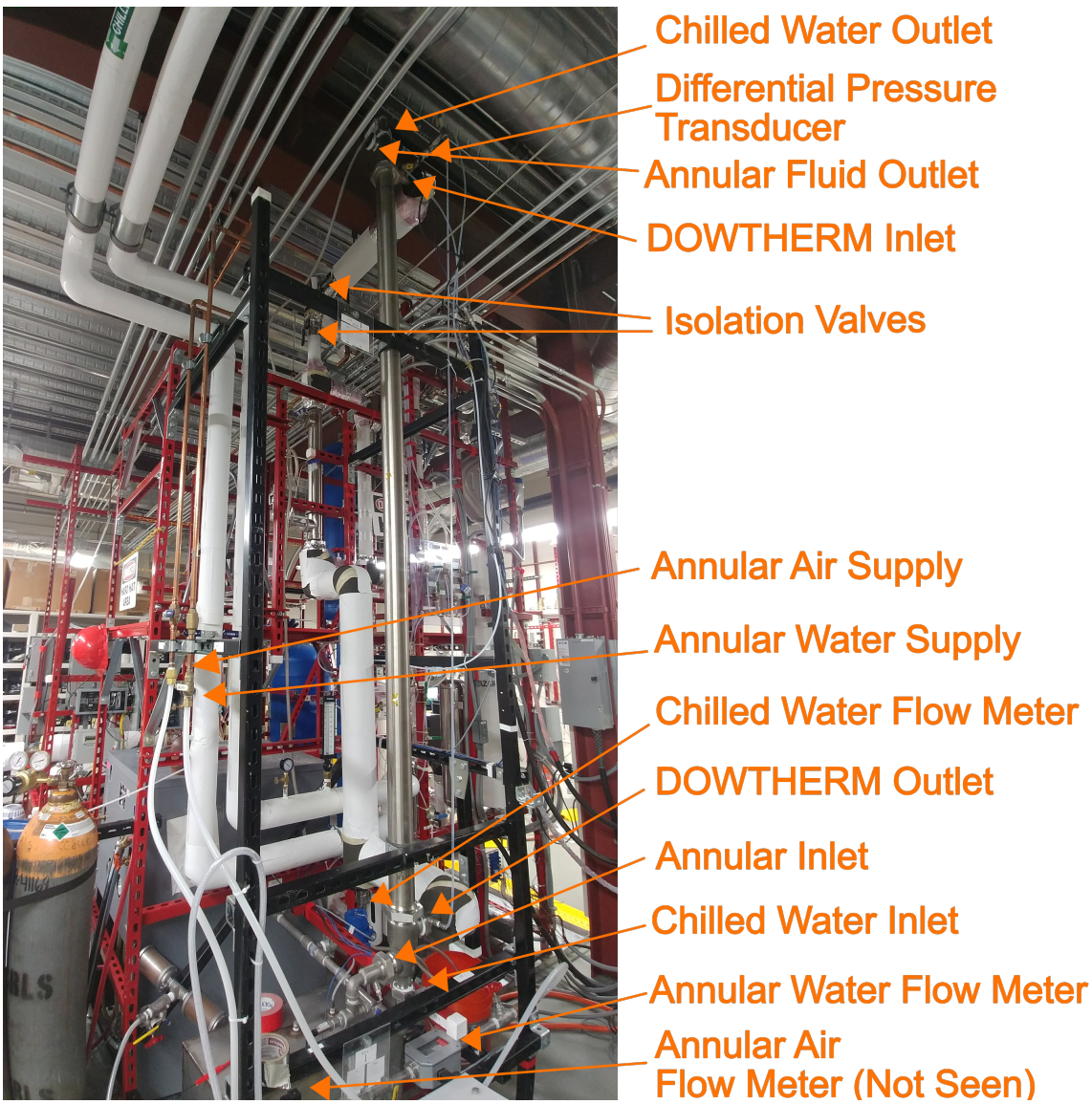

Figure 4.2: Labeled photo of the double-wall heat exchanger test section

temperature and flow-rate. After use, the air is expelled at the top of the facility through two air suppressors and the water is discharged into a floor drain.

Updates to the facility not only had to be physical but updates to the LabView PID system were also necessary. The change of the test section and control meant that the PID system no longer adequately controlled temperature set point of the new

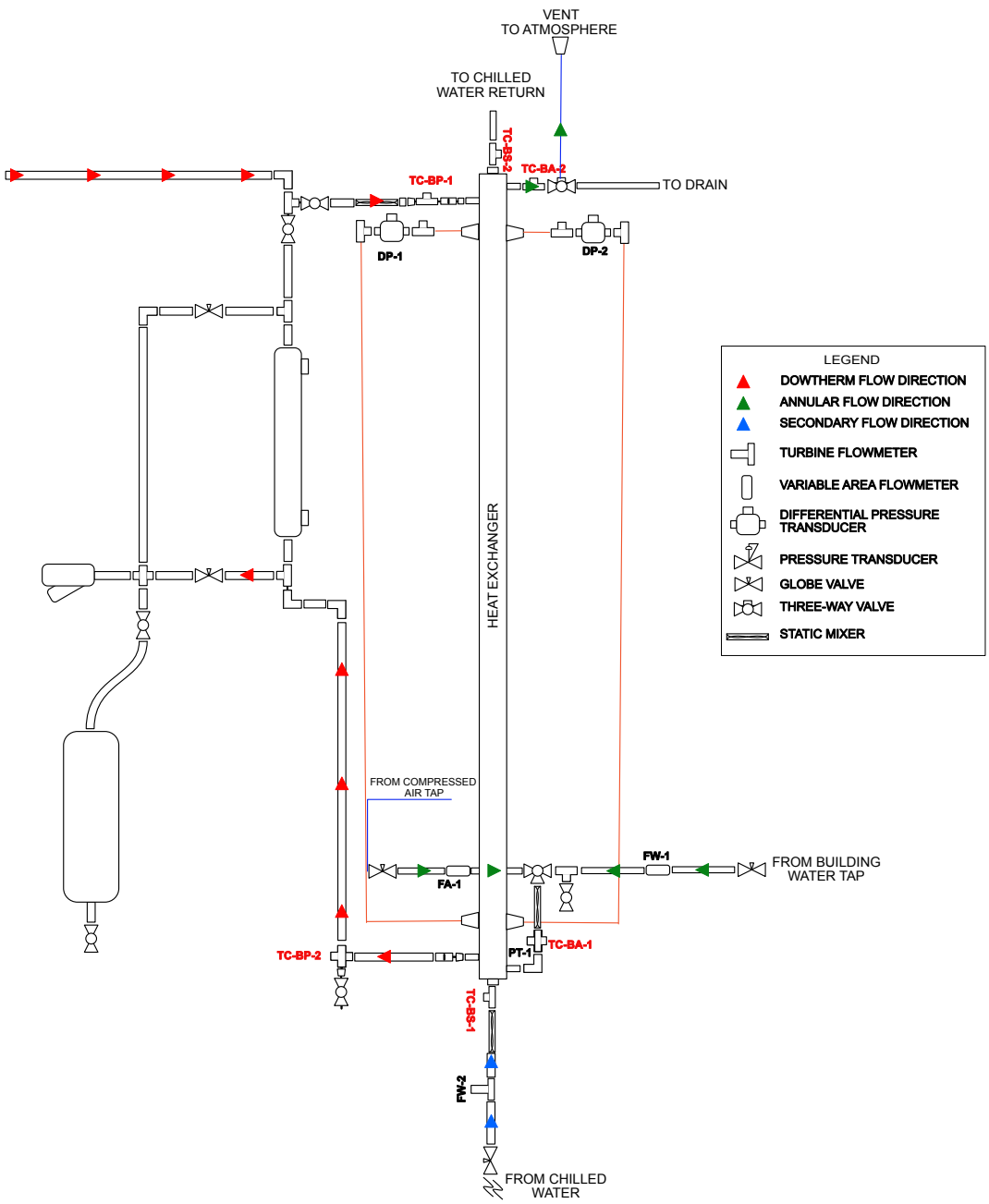

Figure 4.3: Schematic of the addition to the HTF

test section. PID systems typically control electronic systems with quick response times on the order of a few seconds or minutes. The HTF, however, operates on time

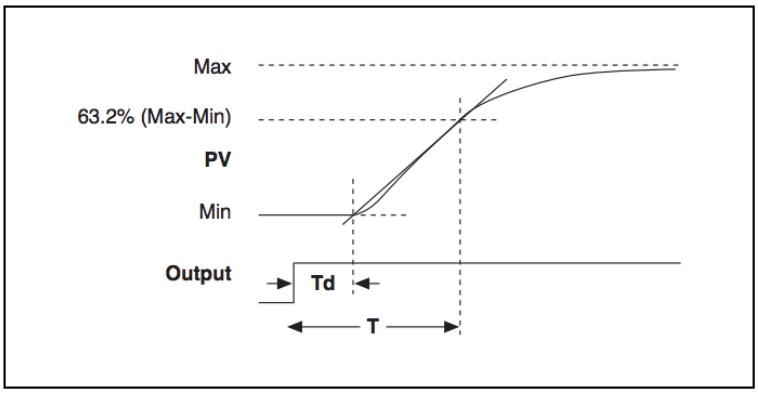

Figure 4.4: Output and Process Variable Chart

Table 4.1: Determination of PID parameters

Controller	PB (Percent)	Reset (minutes)	Rate (minutes)
P	$100KT_d/T$	-	-
PI	$110KT_d/T$	$3.33T_d$	-
PID	$80KT_d/T$	$2.00T_d$	$0.50T_d$

scales significantly longer. It can take upwards of a few hours for the facility to reach the temperature set point. Typical methods for tuning a PID controller are based on an iterative procedure. Attempts for this type of procedure would require significant amounts of time. An alternative procedure was found known as the Open-Loop or Step Test Tuning Procedure. With the controller in a manual mode, the output is set to a nominal value and the response allowed to settle. A step change in the output is then made. After the response settles again, values for the PID can be derived from the following figure:

where T_d is the deadtime in minutes, T is the time constant in minutes and $K = \frac{Change\ in\ Process\ Variable}{Change\ in\ Output}$.

Using this method, new values for the controller were found as $P = 140.6$, $I = 10$, $D = 2.5$.

4.2 Experimental Approach

Similar to tests done for the shell-and-tube heat exchangers, the average temperature through the heat exchanger was set from $60°C - 90°C$. The flow rate for the shell-side fluid was easily adjusted through the operating range of the pump. The intermediate and tube-side fluids were not as easy to change. Relying on building supply made the design of the updates easy however, the supplied fluid flow, temperature, and pressure can fluctuate to some degree without notice. Globe valves on these streams were generally able to throttle flow to the desired flow rate. Inlet temperatures were out of our control however.

This work is interested in the effect that the intermediate fluid has on the effectiveness of the heat exchanger as well as validating a tool for determining the temperature distributions of each of the three fluids for predicting future performance of three-fluid heat exchangers. As such, the approach for experimental conditions were two-fold. The first, was to slow flow rates for the shell-side and tube-side fluids to achieve a temperature difference of $10°C$ between each fluid's inlet and outlet temperature. This was done while varying the flow rate and fluid type of the intermediate fluid. This method was chosen because a larger temperature difference gives more confidence in heat transfer results. The second method used was similar to the one described in the previous chapter with the target fluid always being annular fluid and the tube-side and shell-side fluids were ran as fast as possible to minimize their resistance to heat transfer.

It is important to note that as testing went on, the experimental approach was changed due to a number of circumstances. The first change was due to relying on the building chilled water supply. Though typically not used for experimental work, exceptions are often made to use this water supply. While known that the system was intended for use in building cooling at the university, it was unknown at the

time of experimental design that the university reduces the pressure differential of the supply during the winter. This reduced the maximum flow rate of the supply by half. While changing experimental conditions during the experiment is not ideal, this change should have little impact on the goals of this experiment.

Another change happened with the annular air flow. In designing the experiment it was understood that the compressed air was pressurized well above 100 psi. The design of the experiment was to use air compressed to 100 psi with different flow rates through the test section. This however, was not the case and the air supply was found to be compressed at 100 psi. Therefore, initial estimates for heat transfer were not valid as experimentally, the test section was pressurized lower than this in order to achieve adequate flow. Along with this finding, corrections to the variable area flow meter needed to be applied as the meter is intended for measuring flow of compressed air at 100 psi. The manufacturer provided correlations based on temperature, specific gravity, and pressure.

A third and final change needed to be applied due to the nature of the experimental system. The double-wall test section was added to the secondary side of the HTF. This meant that in order for heat to reach the test section, it must first be added to the primary side fluid through the electrical resistance heater and then must be transferred to the secondary side through the primary heat exchanger. Due to limitations in this heat exchanger and losses through the insulation on the primary and secondary sides, the maximum heat transfer to the secondary side was significantly smaller than the facility is rated for. The primary and secondary loops were insulated in 1" thick glass insulation. The additions for accommodating the double-wall heat exchanger increased the thickness of insulation to 2" to reduce facility heat loss. In tests with high shell-side flow rate and high temperature set point with high water annular flow rate, heat lost to the chilled water and annular water were greater than could be provided through the primary heat exchanger. This lead to the sys-

tem never reaching the testing set point. In these cases, the shell-side flow rate was reduced increasing the resistance to heat transfer in the heat exchanger. These cases were significantly more prominent when the twisted annular tube was tested thus qualitatively giving us results that the twisted tube transferred significantly more heat for the same experimental conditions.

The approach for determining fluid flow direction used the 3FHE solver found in Appendix A. This solver is based off of the theory found in Sekulic [12] and described in Chapter 2. There are four possible flow configurations, shown in Figure 2.1, in a heat exchanger of this type. The chosen configuration is that of P3 and was chosen for two reasons. The first is that ultimately from fluid 1 to fluid 3 the heat exchanger operates in a counterflow configuration from heat source to sink. The second is that this configuration avoids a phenomenon knows as temperature cross. In two-fluid exchangers this is defined to exist when the cold fluid outlet temperature is hotter than the hot fluid outlet temperature. The hot fluid is then gaining heat after the temperature cross resulting in wasted heat transfer area. The phenomenon can also happen in a three-fluid heat exchanger where the hot fluid directly transfers heat to either one or both cold fluids.

4.3 Results

This section shows the results of the SADWPT and SADWTT heat exchangers. The results shown are based on the effectiveness of the heat exchanger, a metric which was described in chapter 2. It is important to note that the effectiveness of the heat exchanger is a flawed metric. The effectiveness is heavily influenced by the outlet temperatures of the three fluids. As these fluid temperatures approach each other, the effectiveness itself will increase. Therefore, for tests utilizing the first method of experimentation with slow flow rates in the shell-side and tube-side fluids, the

absolute magnitudes shown will be higher than those of the tests using the other method. In the following figures, the absolute magnitude of the effectiveness is not of sole interest but the trend of the effectiveness is important as well. The absolute magnitude is used in comparison between the two heat exchangers, the plain and twisted tube.

Effectiveness

Plain Intermediate Tube

Figures 4.5 through 4.7 show the results of the plain tube tests with water as the intermediate fluid. Figure 4.5 shows the effect that the change in the flow rate of the intermediate fluid has on the overall effectiveness of the heat exchanger. Similarly, in figures 4.6 and 4.7 the impact of the change in flow rate on the temperature effectiveness of the intermediate and secondary fluids is shown.

Figures 4.8 through 4.10 show the results of the plain tube tests with compressed air as the intermediate fluid. It is important to note that these air results should be taken with a grain of salt. No matter the testing method, there was very little heat transferred between the three fluids. The author's confidence in these results is therefore small. Suggestions for testing with air can be found in chapter 5.

Twisted Intermediate Tube

Figures 4.11 through 4.13 show the results of the twisted tube with water as the intermediate fluid.

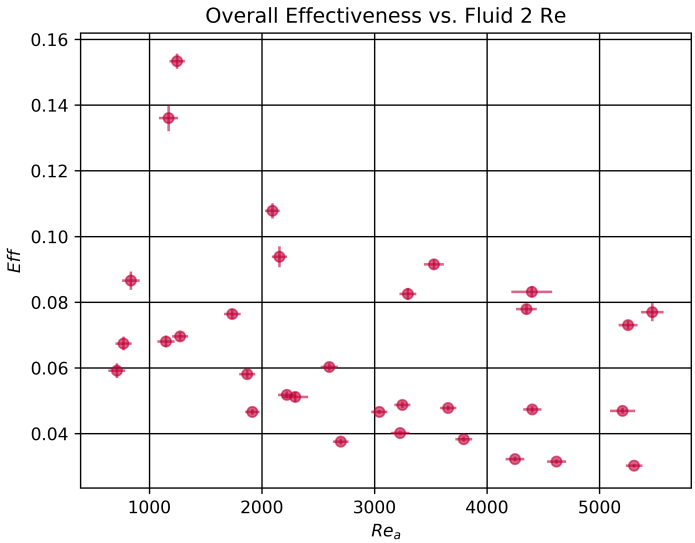

Figure 4.5: The overall effectiveness of the plain tube heat exchanger decreases as the flow of water in the annular region increases

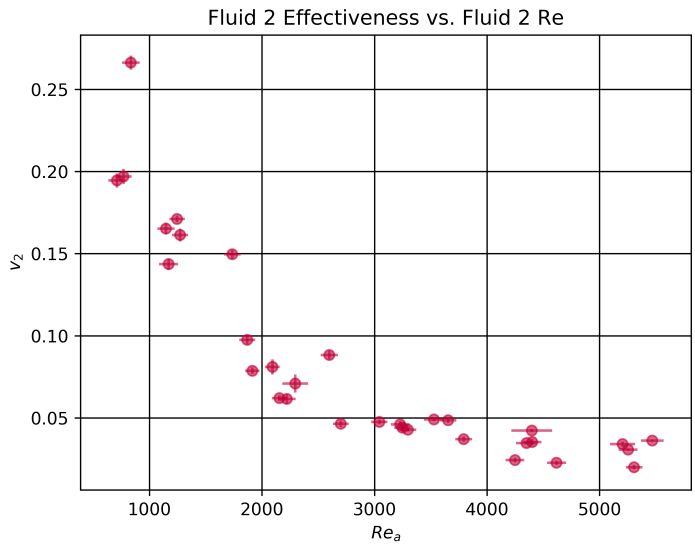

Figure 4.6: The temperature effectiveness of fluid 2 decreases as the flow of water in the annular region increases

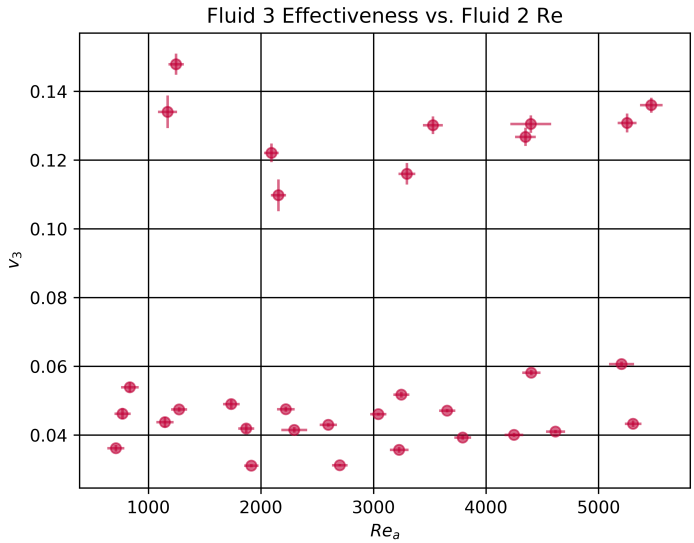

Figure 4.7: In the studied region, the temperature effectiveness of the third fluid has little response to changes in the flow of the annular water

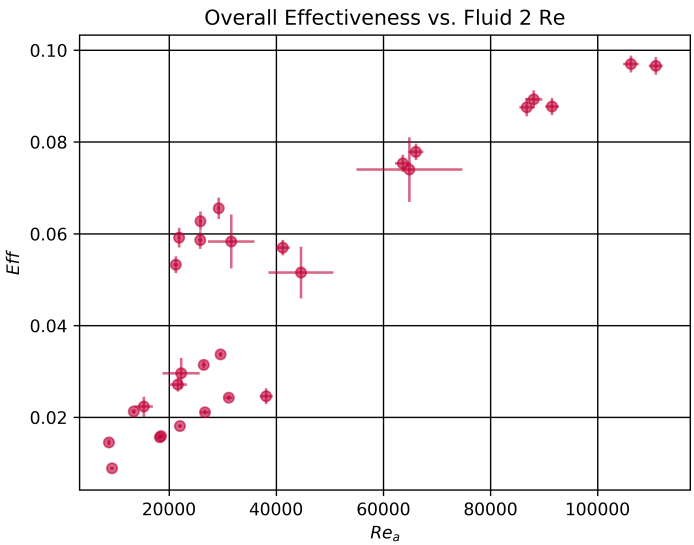

Figure 4.8: Overall effectiveness of the plain tube heat exchanger increases as the flow of air in the annular region increases

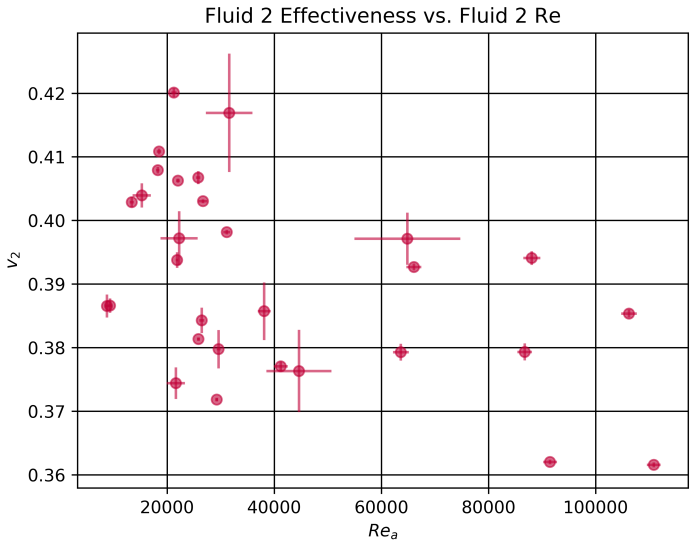

Figure 4.9: The temperature effectiveness of fluid 2 decreases as the flow of air increases

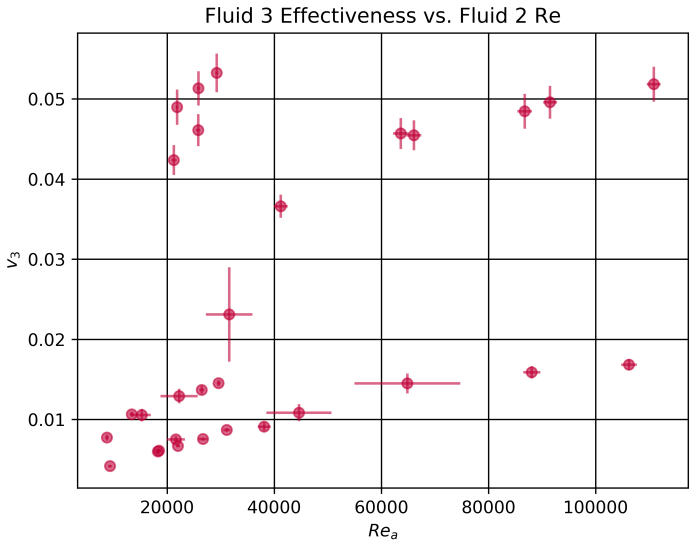

Figure 4.10: Temperature effectiveness of fluid 3 increases as the flow of air increases in this region

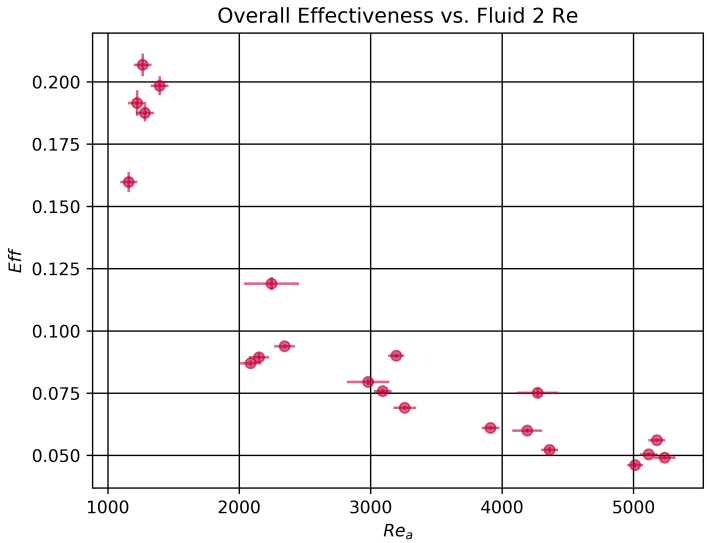

Figure 4.11: Effectiveness of the Twisted tube heat exchanger also decreased as the flow of water increased

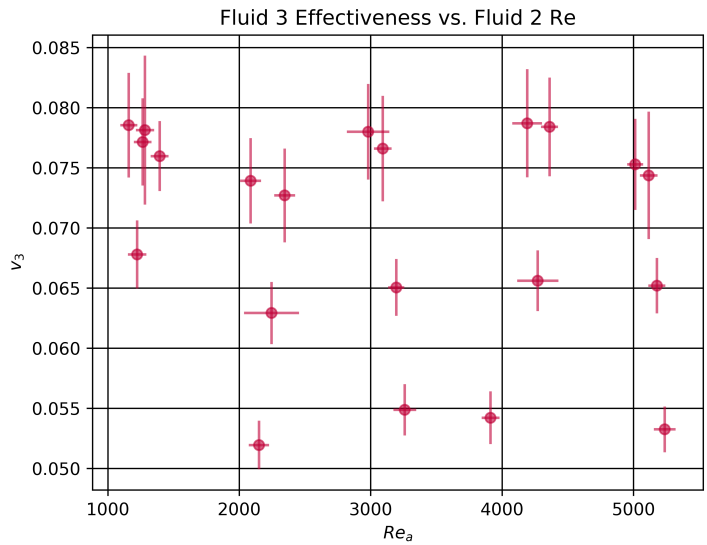

Figure 4.12: The temperature effectiveness of the fluid 3 has a small response, a slight decrease in the effectiveness as the flow of water in the annular region increases

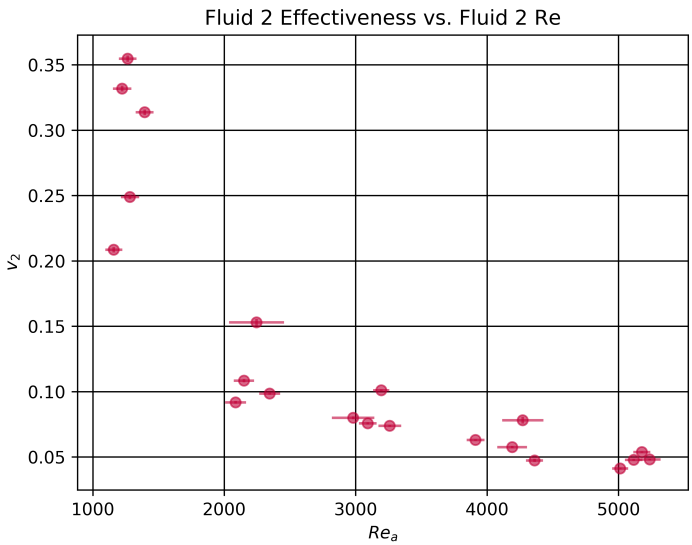

Figure 4.13: As expected, the temperature effectiveness of fluid 2 decreases as the flow increases

Table 4.2: Experimental parameters chosen for comparing predicted and measured values

	Shell-Side Flow Rate (GPM)	Intermediate Flow Rate (GPM)	Tube-Side Flow Rate (GPM)	Shell-Side Inlet Temperature $°C$	Intermediate Inlet Temperature $°C$	Tube-Side Inlet Temperature $°C$
Case 1	2.08 ± 0.02	4.79 ± 0.4	0.292 ± 0.2	87.8 ± 0.2	25.6 ± 0.2	8.05 ± 0.2
Case 2	9.66 ± 0.05	1.77 ± 0.4	3.04 ± 0.1	64.5 ± 0.2	25.8 ± 0.2	61.5 ± 0.2
Case 3	6.35 ± 0.05	2.34 ± 0.4	2.78 ± 0.1	82.7 ± 0.2	28.8 ± 0.2	5.97 ± 0.2

Tool Validation

Three experimental points were chosen from the water tests performed with the plain tube heat exchanger. The testing conditions were then replicated in the 3FHE code. The three testing conditions are displayed in Table 4.2. The resulting temperature distributions are shown in figures 4.14-4.16.

Table 4.3: Comparison between measured and predicted values for Case 1

Case 1	Shell-Side Outlet Temperature	Intermediate Outlet Temperature	Tube-Side Outlet Temperature
Measured Values	72.5 ± 0.2	27.9 ± 0.2	18.9 ± 0.2
Predicted Values	76.6	27.2	15.5
Percent Difference	5.7	2.5	18

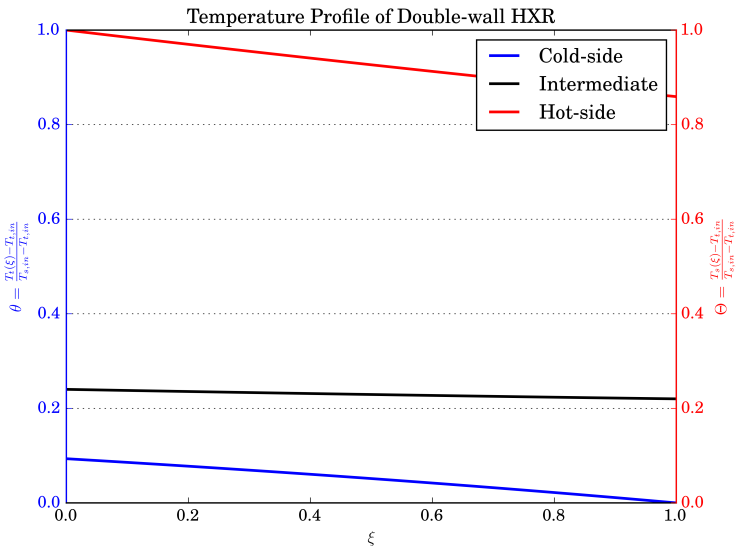

Figure 4.14: Predicted temperature distribution for Case 1

Table 4.4: Comparison between measured and predicted values for Case 2

Case 2	Shell-Side Outlet Temperature	Intermediate Outlet Temperature	Tube-Side Outlet Temperature
Measured Values	58.6 ± 0.2	28.0 ± 0.2	9.01 ± 0.2
Predicted Values	56.8	32.9	8.3
Percent Difference	3	18	7.9

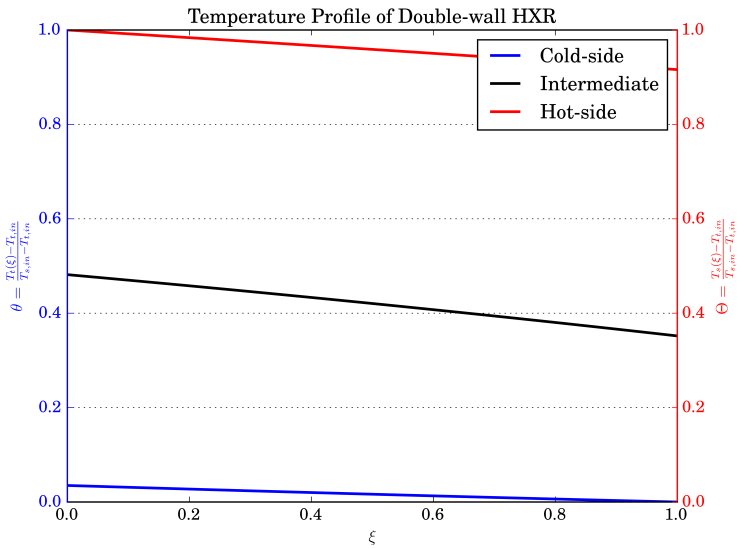

Figure 4.15: Predicted temperature distribution for Case 2

Table 4.5: Comparison between measured and predicted values for Case 3

Case 3	Shell-Side Outlet Temperature	Intermediate Outlet Temperature	Tube-Side Outlet Temperature
Measured Values	77.0 ± 0.2	31.3 ± 0.2	9.53 ± 0.2
Predicted Values	74.4	34.2	9.4
Percent Difference	3.3	9.2	1.4

4.4 Discussion and Conclusion

As shown in figure 4.5 there is a clear trend in the overall effectiveness of the plain tube heat exchanger. As the flow of water in the annular space increases, the overall effectiveness of the heat exchanger decreases. Qualitatively, this phenomenon can be attributed to the increasing rate of the intermediate fluid removing more heat than it is passing on to the tube-side fluid. Given the limitations of our facility, we can not

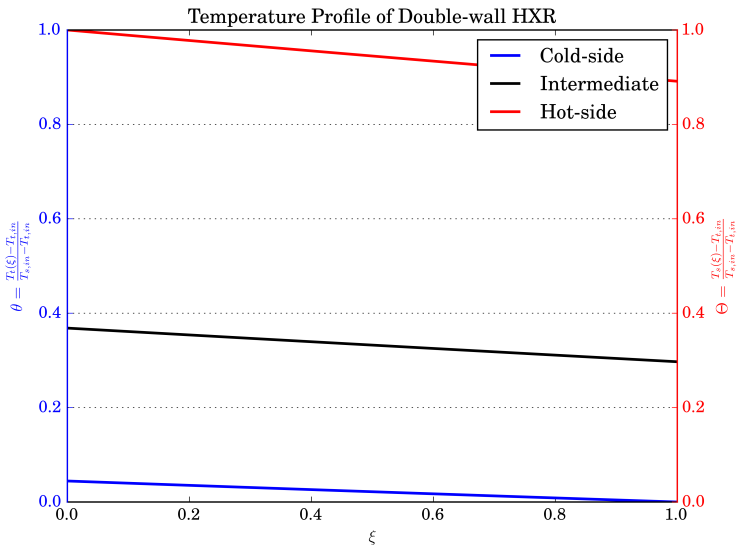

Figure 4.16: Predicted temperature distribution for Case 3

slow the intermediate water any more with high confidence in our flow measurement to find a possible maximum point of effectiveness.

In examining figure 4.8, the opposite trend appears in the overall effectiveness. As the flow of air increases, the overall effectiveness increases as well. It appears that with a greater convective heat transfer coefficient, the air is better able to transfer heat to the tube-side fluid. The question then becomes, is there a point at which the air begins to act like the water in the annular region and the overall effectiveness will begin to decrease as the flow rate continues to increase.

Figure 4.11 shows the experiments for the twisted annular tube. Here we see a similar trend where the effectiveness decreases as the flow rate increases. However, looking at the absolute magnitude of the effectiveness it is clear that the twisted tube increases the effectiveness of the heat exchanger when compared to the plain tube under similar experimental conditions.

Tables 4.3-4.5 show the comparison of the results for the experimental tests as

well as those which were predicted with the energy balance equation. As seen, the predicted method performed best in calculating the outlet temperature for the shell-side fluid. Predicting the outlet temperatures for the intermediate and tube-side fluids was harder, averaging 10 and 9 percent off from the actual values respectively. These high errors are notably due to the difficulty in predicting heat transfer coefficients of fluids. In a guess-and-check estimate to minimize the difference between calculated and measured values, it was found that given more accurate NTUs for the fluids resulted in significantly more accurate results, under a 5 percent difference from measured values.

Chapter 5

Future Work

Chapter 4 performed initial experimental studies for scoping 3FHEs. As seen in the previous chapter, as the flow rate of water as the intermediate fluid increases, the overall effectiveness of the heat exchanger decreases. Is there a maximization point, where the effectiveness will start to decrease with decreasing flow rate? Another question is for air as the annular fluid, is there a point where the air begins to act similarly to water as the intermediate fluid?

The funding for this work has come from a variety of sources including the Department of Energy Integrated Research Project and Nuclear Energy University Program (NEUP). Conditions for the NEUP require testing of a double-wall heat exchanger design at Sandia National Laboratory(SNL). Future work for this project relies on the facilities at SNL including the use of their supercritical carbon dioxide (SCO2) loop. This experiment will focus on the coupling of FHR systems to SCO2 Brayton cycle systems for energy production. As the demand for more efficiency and safety goes up, the nuclear field must be able to take advantage of technological advances such as using Brayton cycle systems. Given the validation of the tool for calculating the temperature distributions for a parallel stream three fluid heat exchanger, the

performance for the three fluid tube bundle heat exchangers can be estimated. The estimates will be useful in determining experimental conditions for testing at Sandia.

As this author pointed out in Chapter 4, heat transfer using air was extremely poor and resulted in very low confidence in the results. It is suggested that those who will continue this work at Sandia create a closed loop of air or helium in the annular space. The ability to more finely control the pressure and flow rate of the annular fluid will greatly increase confidence in results. It is suggested that the testing pressure for air meets or exceeds 100psi as the relevant thermophysical properties are significantly better for heat transfer for the small scale testing.

Ultimately, the author sees this work being used in conjunction with appropriate mass transfer studies. Optimization of a three fluid heat exchanger can then take place, the maximization of tritium removal and heat transfer can take place for a given three fluid heat exchanger design. Appropriate mass transfer studies could determine the time for tritium to migrate through the annular space and thus determine a minimum flow rate required to remove adequate amounts of tritium from the heat exchanger. The use of the 3FHE tool can be used to maximize the heat transfer to the power generation fluid.

Chapter 6

Summary

The work described here characterizes multiple scaled experiments in the space of advanced heat exchanger design for the FHR. As noted, the FHR has multiple flaws based on the baseline choice for the molten salt coolant. Flibe as a coolant has a moderately high Prandtl number. In a pool type design such as the Mark-1 PB-FHR, the DRACS heat exchanger constantly operates under natural circulation conditions. The HTF at UNM was designed to perform tests using scaled heat transfer fluid DOWTHERM A. A twisted tube heat exchanger and a plain tube heat exchanger of an identical design and tube size were tested under both natural circulation and forced circulation conditions. As seen in chapter 3, the shell-side fluid had a greater Nusselt number in both natural circulation and forced circulation tests in the twisted tube heat exchanger.

Another issue with flibe is the neutron interactions with the each of the components. Specifically neutron interactions with ^6Li create significant amounts of tritium in the form of T_2 or TF. At the high operating temperatures of the FHR, hydrogen and its isotopes can readily permeate through structural materials especially in areas with large surface areas such as the intermediate heat exchanger and secondary

heat exchanger. A DWHE could be used as a solution to the prevention of tritium permeation to the power generation fluid. The HTF had multiple physical updates to accommodate a single-assembly double-wall heat exchanger, essentially a three fluid heat exchanger. The effectiveness was determined as a metric for measuring the performance of both the plain and twisted intermediate tube heat exchangers. Mixed results were found based on the intermediate fluid as to the effect the change in the Reynolds number has on the overall effectiveness of the heat exchanger.

The single-assembly double-wall heat exchanger was also used to validate a tool for predicting the performance for a three fluid parallel stream heat exchanger with two thermal communications. The three fluid heat exchanger tool can be used to understand and predict the temperature distributions for any parallel stream three fluid heat exchanger. Most specifically for future work to be done at Sandia, this tool can be used to predict heat exchanger performance of two heat exchangers acquired by UNM which are double wall shell and tube heat exchangers with either plain or twisted tube bundles.

Appendix A

Three-Fluid Heat Exchanger Temperature Distribution Program

```
# This code predicts the temperature distribution of the
    SADWPT heat exchanger given the inlet temperatures and
    flow rates of the experiment. NOTE: Predictions for
    Nusselt number vary based on experiment. The user must
    decide which Nusselt correlation to use. The code can be
    used for twisted tube heat exchangers as well. The twisted
     tube effects should be characterized within the
    definition of NTU

import numpy
import matplotlib.pyplot as plt
import matplotlib.lines as mlines
import csv
```

```
from scipy.integrate import odeint, solve_bvp
from scipy.optimize import root, fsolve
import tp_properties
import Nusselt_PT

fig, ax1 = plt.subplots()
ax2 = ax1.twinx()

# NUMBER OF NODES (IMPORTANT FOR CONVERGENCE)

nodes    = 100000

# For air tests include pressure
P =
# DEFINE ABSOLUTE TEMPERATURES

T_1i  =    #inlet temperatures of each fluid stream
T_2i  =
T_3i  =
T_sp  =      #temperature setpoint of experiment

# FLUID 1 IS ALWAYS POSITIVE DIRECTION

# DEFINE FLUID 2 AND 3 DIRECTIONS AS POSITIVE (+1) OR
    NEGATIVE (-1)

i_2    = -1
i_3    = -1
```

```
#Input flow rates
Flow1 =  #gpm
Flow2 =  # For air, need to change flow rate to accomdate
   SCFM
Flow3 =

#Define Thermophysical Properties
[rho1,cp1,mu1,lambda1] = tp_properties.tp_dowtherm(T_sp)
[rho2,cp2,mu2,lambda2] = tp_properties.tp_air(T_2i, P)
[rho3,cp3,mu3,lambda3] = tp_properties.tp_water(T_3i)

#Calculate mass flow rates
mf1 = Flow1*.000063*rho1
mf2 = Flow2*.000063*rho2
mf3 = Flow3*.000063*rho3

# DEFINE HEAT CAPACITY RATES J/sK
C_1    = mf1*cp1*1000 #252
C_2    = numpy.array([mf2*cp2*1000]) #numpy.array([11])
C_3    = mf3*cp3*1000 #105

#SADWTT Areas
A_1 = 0.485 #m^2
A_2 = 0.285  #m^2

#Re Calculations
Re1 = Flow1*.000063*.0153/(mu1/rho1*.000189)
```

```
Re2 = Flow2*.000063*.022/(mu2/rho2*.00051)
Re3 = Flow3*.000063*.028/(mu3/rho3*.000616)

#Pr calculations
Pr1 = cp1*1000*mu1/lambda1
Pr2 = cp2*1000*mu2/lambda2
Pr3 = cp3*1000*mu3/lambda3

#Nu Predictions
Nu1 = Nusselt_PT.Nu_Gnielinski(Re1, Pr1, .0153, 3)
Nu2 = Nusselt_PT.Nu_DittusBoelter(Re2, Pr2)#, .022, 3)
Nu3 = Nusselt_PT.Nu_StefanPreuber(Re3, Pr3, .028, 3)

#Individual heat transfer coefficient calculations from Nu
    predictions
h1 = Nu1*lambda1/.0153
h2 = Nu2*lambda2/.022
h3 = Nu3*lambda3/.0285
#Calculate overall heat transfer coefficients
U_1 = 1/((1/h1) + (.029/16)*numpy.log(.027/.029) +
    (.029/.027)*(1/h2))
U_2 = 1/((1/h2) + (.016/16)*numpy.log(.014/.016) +
    (.016/.014)*(1/h3))
# DEFINE NTU'S
NTU_1    = (U_1*A_1)/C_1 #.088 # DEFINED AS (U_1 A_1)/C_1
NTU_2    = (U_2*A_2)/C_2 #1.86 # DEFINED AS (U_2 A_2)/C_2

print(Nu1,Nu2,Nu3)
```

```
print(h1,h2,h3)
print(C_1,U_1,C_2,U_2,NTU_1,NTU_2,C_3)
print(Re1,Pr1,Re2,Pr2,Re3,Pr3)

# DEFINE INTERMEDIATE INLET TEMPERATURE Non-dimensional

theta_2in = (T_2i-T_3i)/(T_1i-T_3i) #0.17

# DETERMINE HEAT CAPACITY STREAM RATIOS

R_1   = C_1/C_3
R_2   = C_2/C_3

# SOLVE THE BOUNDARY VALUE PROBLEM

for i in range(0,len(C_2)):
  def myfun(x, y):
    return numpy.vstack(( NTU_1*(y[1]-y[0]), i_2*NTU_1*(R_1/
       R_2[i])*(y[0]-y[1])+i_2*NTU_2*(y[2]-y[1]), i_3*NTU_2*
       R_2[i]*(y[1]-y[2]) ))
  def bc(ya, yb):
    residual_1  = ya[0]-1
    if i_2 == 1:
      residual_2  = ya[1]-theta_2in
      #residual_2   = ya[1]-yb[1]
    if i_2 == -1:
      residual_2  = yb[1]-theta_2in
      #residual_2   = yb[1]-ya[1]
```

```
    if i_3 == 1:
      residual_3 = ya[2]
    if i_3 == -1:
      residual_3 = yb[2]
    return numpy.array([ residual_1, residual_2, residual_3
        ])
  x = numpy.linspace(0, 1, nodes)
  y = numpy.zeros((3, x.size))
  sol = solve_bvp(myfun, bc, x, y, max_nodes=1e6, verbose=2
     )

  y0 = sol.sol(x)[0]  # hot temperature
  y1 = sol.sol(x)[1]  # intermediate temperature
  y2 = sol.sol(x)[2]  # cold temperature

  ax1.plot(x, y0, 'r', linewidth=2.0)
  ax1.plot(x, y1, 'k', linewidth=2.0)
  ax2.plot(x, y2, 'b', linewidth=2.0)

# PRINT MEAN TEMPERATURE DIFFERENCES (DETERMINED NUMERICALLY
    - MUST CHECK FOR CONVERGENCE MANUALLY)

MTD_1to2_numerical  = numpy.mean(y0-y1)
MTD_2to3_numerical  = numpy.mean(y1-y2)
MTD_1to3_numerical  = numpy.mean(y0-y2)


print("")
```

```
print("MTD_1to2_numerical \t= {:4.4f} \t= {:4.1f} C".format(
    MTD_1to2_numerical,MTD_1to2_numerical*(T_1i-T_3i)))
print("MTD_2to3_numerical \t= {:4.4f} \t= {:4.1f} C".format(
    MTD_2to3_numerical,MTD_2to3_numerical*(T_1i-T_3i)))
print("MTD_1to3_numerical \t= {:4.4f} \t= {:4.1f} C".format(
    MTD_1to3_numerical,MTD_1to3_numerical*(T_1i-T_3i)))
print("")
print("T_1o  \t\t\t= {:4.4f} \t= {:4.1f} C".format(y0[x.size
    -1],y0[x.size-1]*(T_1i-T_3i)+T_3i))
T_1o = y0[x.size-1]*(T_1i-T_3i)+T_3i
if i_2 == 1:
  print("T_2o  \t\t\t= {:4.4f} \t= {:4.1f} C".format(y1[x.
      size-1],y1[x.size-1]*(T_1i-T_3i)+T_3i))
  T_2o = y1[x.size-1]*(T_1i-T_3i)+T_3i
if i_2 == -1:
  print("T_2o  \t\t\t= {:4.4f} \t= {:4.1f} C".format(y1[0],
      y1[0]*(T_1i-T_3i)+T_3i))
  T_2o = y1[0]*(T_1i-T_3i)+T_3i
if i_3 == 1:
  print("T_3o  \t\t\t= {:4.4f} \t= {:4.1f} C".format(y2[x.
      size-1],y2[x.size-1]*(T_1i-T_3i)+T_3i))
  T_3o = y2[x.size-1]*(T_1i-T_3i)+T_3i
if i_3 == -1:
  print("T_3o  \t\t\t= {:4.4f} \t= {:4.1f} C".format(y2[0],
      y2[0]*(T_1i-T_3i)+T_3i))
  T_3o = y2[0]*(T_1i-T_3i)+T_3i
print("")
```

```
with open('PyDoubleWallOutput.csv','w') as f:
    writer = csv.writer(f)
    writer.writerow(['T_1i', 'T_3i', 'NTU_1','NTU_2','C_1','
        C_2','C_3','theta_2in','T_1o','T_2o','T_3o'])
    writer.writerow([T_1i,T_3i,NTU_1,NTU_2,C_1,C_2,C_3,
        theta_2in, T_1o, T_2o, T_3o])

R_3 = C_2/C_1
R_4 = C_3/C_1
#R_4*(y2[0] - y2[1]) + R_3*y0[1])

stream3eff = y2[0]
stream2eff = (y1[0]-theta_2in)/(1-theta_2in)

print("stream3eff = ", stream3eff)
print("stream2eff = ", stream2eff)

effectiveness = (R_3*stream2eff*(1-theta_2in) + R_4*
    stream3eff)/(R_3*(1-theta_2in) + R_4)

print("overall effectiveness = ", effectiveness)

# FINISH PLOTTING

plt.rc('text', usetex=True)
plt.rc('font', family='serif')
ax1.set_xlabel('$\\xi$')
```

```
ax1.set_ylabel('$\\theta = \\frac{T_t(\\xi)-T_{t,in}}{T_{s,
    in}-T_{t,in}}$', color='b')
ax1.set_xlim([0,1])
ax1.set_ylim([0,1])
ax1.tick_params(axis='y', color='b', labelcolor='b')
ax2.set_ylabel('$\\Theta = \\frac{T_s(\\xi)-T_{t,in}}{T_{s,
    in}-T_{t,in}}$', color='r')
ax2.set_ylim([0,1])
ax2.tick_params(axis='y', color='r', labelcolor='r')
ax2.spines['left'].set_color('b')
ax2.spines['right'].set_color('r')
plt.title('Temperature Profile of Double-wall HXR')
blue_line = mlines.Line2D([], [], linewidth=2.0, color='blue
    ', label='Cold-side')
red_line = mlines.Line2D([], [], linewidth=2.0, color='red',
     label='Hot-side')
black_line = mlines.Line2D([], [], linewidth=2.0, color='
    black', label='Intermediate')
plt.legend(handles=[blue_line, black_line, red_line], loc='
    best')
plt.grid(True)
plt.savefig('double_wall_hxr.png',dpi=600,format='png')
plt.show()
```

References

[1] H. Schlichting, *Boundary-Layer Theory*. 1979.

[2] D. F. Williams, L. Toth, and K. Clarno, "Assessment of Candidate Molten Salt Coolants for the AHTR," Tech. Rep. June, Oak Ridge National Laboratory, Oak Ridge, Tennessee, 2006.

[3] H.-t. R. P.-f. P. Plant, A. Y. K. Chong, K. D. Huff, D. L. Krumwiede, and M. R. Laufer, "Mark -- 1 PB -- FHR Technical Description Technical Description of the "Mark 1" Pebble-Bed Fluoride-Salt-Cooled High-Temperature Reactor (PB-FHR) Power Plant," pp. 1–153, 2014.

[4] J. D. Stempien, R. G. Ballinger, and C. W. Forsberg, *Tritium Transport and Corrosion Modeling in the Fluoride Salt-Cooled High-Temperature Reactor*. Phd dissertation, Massachusetts Institute of Technology, 2015.

[5] L. Gilman and C. Forsberg, "Optimum Double-Wall Heat Exchanger for Containment and Trapping of Tritium in a Salt-Cooled Reactor," in *Transactions of the American Nuclear Society*, vol. 109, pp. 1071–1074, 2013.

[6] S. R. Sherman and T. M. Adams, "Tritium Barrier Materials and Separation Systems for the NGNP," Tech. Rep. November, Savannah River National Laboratory, 2008.

[7] K. Forcey and D. Ross, "The formation of hydrogen permeation barriers on steels by alumising," *Journal of Nuclear Materials*, vol. 182, pp. 36–51, 1990.

[8] J. T. Hughes, *Experimental and Computational Investigations of Heat Transfer Systems in Fluoride Salt-cooled High-temperature Reactors*. Phd dissertation, University of New Mexico, 2017.

[9] C. T. Crowe, D. F. Elger, and J. A. Robertson, *Engineering Fluid Mechanics*. 2005.

[10] S. Chruchill, "Friction Factor Equations Spans all Fluid-Flow Regimes," *Chemical Engineering (New York)*, vol. 84, no. 24, pp. 91–92, 1997.

[11] T. L. Bergman, A. Lavine, F. P. Incropera, and D. P. Dewitt, *Fundamentals of Heat and Mass Transfer*. 2011.

[12] D. Sekulic and R. Shah, "Thermal Design Theory of Three-Fluid Heat Exchangers," *Advances in Heat Transfer*, vol. 26, pp. 219–324, 1995.

[13] P. M. Bardet and P. F. Peterson, "Options for scaled experiments for high temperature liquid salt and helium fluid mechanics and convective heat transfer," *Nuclear Technology*, vol. 163, no. 3, pp. 344–357, 2008.